

Adaptive Multi-View ICA: Estimation of noise levels for optimal inference

Hugo Richard
Inria, Université Paris-Saclay
Saclay, France
hugo.richard@inria.fr

Pierre Ablin
Département de Mathématiques et Applications
Ecole Normale Supérieure
Paris, France
pierre.ablin@ens.fr

Aapo Hyvärinen
Inria, Université Paris-Saclay, Saclay, France
Department of Computer Science HIIT, University of Helsinki, Finland
aapo.hyvarinen@helsinki.fi

Alexandre Gramfort
Inria, Université Paris-Saclay
Saclay, France
alexandre.gramfort@inria.fr

Bertrand Thirion
Inria, Université Paris-Saclay
Saclay, France
bertrand.thirion@inria.fr

February 23, 2021

Abstract

We consider a multi-view learning problem known as group independent component analysis (group ICA), where the goal is to recover shared independent sources from many views. The statistical modeling of this problem requires to take noise into account. When the model includes additive noise on the observations, the likelihood is intractable. By contrast, we propose Adaptive multiView ICA (AVICA), a noisy ICA model where each view is a linear mixture of shared independent sources with additive noise on the sources. In this setting, the likelihood has a tractable expression, which enables either direct optimization of the log-likelihood using a quasi-Newton method, or generalized EM. Importantly, we consider that the noise levels are also parameters that are learned from the data. This enables sources estimation with a closed-form Minimum Mean Squared Error (MMSE) estimator which weights each view according to its relative noise level. On synthetic data, AVICA yields better sources estimates than other group ICA methods thanks to its explicit MMSE estimator. On real magnetoencephalography (MEG) data, we provide evidence that the decomposition is less sensitive to sampling noise and that the noise variance estimates are biologically plausible. Lastly, on functional magnetic resonance imaging (fMRI) data, AVICA exhibits best performance in transferring information across views.

1 Introduction

Unsupervised multiview learning aims at extracting some shared information from a collection of datasets. In practice, each view contributes a different amount of information. A canonical example is in neuroimaging, where one is interested in recovering a common source from a group of subjects performing the same task. In this setting, a view is given by the brain recording —e.g. magneto-encephalography (MEG) or functional magnetic resonance imaging (fMRI)— of one subject of a group. However, the magnitude of the response differs across subjects, i.e. data exhibit random effects Penny & Holmes (2007). Moreover, the noise level associated with head movements, breath or heart beats is subject-specific and also depends on the brain region considered Liu (2016).

Independent component analysis Comon (1994); Hyvärinen & Oja (2000) (ICA) is a widely used technique to recover independent components from a given signal. ICA has many applications such as finance Chen et al. (2007), astronomy Maino et al. (2002), telecommunications Ristaniemi (1999) or bioinformatics Liebermeister (2002). When ICA is used in a neuroimaging context, the unsupervised multiview learning problem of recovering

common sources from multiple (possibly noisy) mixtures is called *group ICA*. Most popular group ICA methods, routinely used to extract shared responses from neuroimaging data, do not optimize a proper likelihood Calhoun et al. (2001); Varoquaux et al. (2009). Other works Richard et al. (2020); Guo & Pagnoni (2008) have introduced well principled models. However, Richard et al. (2020) assume identical noise variance across sources and views and Guo & Pagnoni (2008) assume identical noise covariance across views. Lastly, in noisy mixtures, the optimal sources estimates are not given simply by inverting the mixing matrices Hyvärinen (1998) and they are often impossible to evaluate in closed-form.

In this paper, we introduce AVICA, a principled method that models multiview data as a linear mixture of sources with additive Gaussian noise on the sources. Importantly, AVICA allows for different noise variances depending on the sources and the views. We show that AVICA is identifiable, and it has a closed-form likelihood as well as a closed-form solution for the E-step in the Expectation-Maximization (EM) algorithm. We introduce two methods for maximizing the likelihood: direct likelihood maximization via an alternating quasi-Newton method and a quasi-Newton EM algorithm. We derive a closed-form minimum mean square error (MMSE) estimate for the sources which allows for finer source estimation. Lastly, we benchmark AVICA on an extensive set of experiments involving synthetic and real data based on two different neuroimaging modalities. On MEG data, we show that the recovered sources are more stable across trials and that the estimated noise variances correlate with the recorded noise level without stimulus. On fMRI data, AVICA exhibits the best performance in predicting the data of a left-out subject.

2 Adaptive multiViewICA (AVICA)

Notation The absolute value of the determinant of a matrix W is $|W|$. The ℓ_2 norm of a vector \mathbf{s} is $\|\mathbf{s}\|$. We define the ℓ_∞ norm of a matrix G by $\|G\|_\infty = \max_{i,j} |G_{ij}|$. The probability density function of the normal distribution with mean μ and variance σ^2 is denoted $x \mapsto \mathcal{N}(x; \mu, \sigma^2)$.

2.1 Model and likelihood

We assume that we have m different *views* associated with a common set of events. AVICA models the data of each view as a weighted combination of noisy sources. The sources are common to each view and constitute the *shared sources*. Denoting $\mathbf{x}^i \in \mathbb{R}^k$ a random vector of data for view i and $\mathbf{s} \in \mathbb{R}^k$ a random vector of shared sources, the model reads:

$$\begin{aligned} \mathbf{x}^i &= A^i(\mathbf{s} + \mathbf{n}^i), \quad i = 1, \dots, m \\ p(\mathbf{s}) &= \prod_{j=1}^k \delta(s_j) \\ \mathbf{n}^i &\sim \mathcal{N}(0, \Sigma^i) \\ \Sigma^i &= \text{diag} \left(\frac{(\sigma_1)^2}{m(\lambda_1^i)^2} \dots \frac{(\sigma_k)^2}{m(\lambda_k^i)^2} \right) \\ \forall j, \sum_{i=1}^m (\lambda_j^i)^2 &= 1 \end{aligned} \tag{1}$$

where $A^i \in \mathbb{R}^{k \times k}$ are unknown *mixing matrices* for each of the m views, and \mathbf{n}^i correspond to some additive noises on the sources. The k shared sources \mathbf{s} are assumed independent with density δ . Finally, the noise terms $\mathbf{n}^1 \dots \mathbf{n}^m$ are assumed to be independent across the m views, and independent from the shared sources.

Considering a Gaussian assumption on the noise of the source j , we parametrize its variance as $\Sigma_j^i = \frac{(\sigma_j)^2}{m(\lambda_j^i)^2}$, where $(\sigma_j)^2$ is the *global noise level* of source j , and $(\lambda_j^i)^2$ is the *relative noise precision* for view i . Σ^i models the deviation between the best possible source estimate one can recover from view i and the shared sources. For a given source j , the relative noise precisions are normalized so that they sum to one, $\sum_i (\lambda_j^i)^2 = 1$. Intuitively, $(\lambda_j^i)^2$ quantifies the influence of view i on source j . The parametrization using $(\lambda_j^i)^2$ and $(\sigma_j)^2$ instead of Σ_j^i yields no loss of generality and its interest will become clear later.

The noise model of AVICA is equivalent to having noise on the sensors with covariance $A^i \Sigma^i (A^i)^\top$, where Σ^i is a diagonal matrix. As the noise variance is inferred from the data, it is a generalization of Richard et al. (2020) in which the noise level is fixed and constant over views and sources. Indeed for each source j and view i , the relative noise precisions $(\lambda_j^i)^2$, the global noise level $(\sigma_j)^2$ and the mixing matrices A^i are estimated.

The following proposition states that the AVICA model has the same permutation and scaling indeterminacies as standard single-view ICA (see appendix B.1 for the proof).

Proposition 1 (Identifiability of Adaptive multiView ICA). *Let \mathbf{x}^i , $i = 1 \dots m$ be generated from equation (1) with parameters $(A^i, \Sigma^i)_{i=1}^m$ and density δ . Assume that there exist parameters $(A'^i, \Sigma'^i)_{i=1}^m$ and density δ' such that $\mathbf{x}^i = A'^i(\mathbf{s}' + \mathbf{n}'^i)$ with $p(\mathbf{s}') = \prod_{j=1}^k \delta'(s'_j)$ and $\mathbf{n}'^i_j \sim \mathcal{N}(0, \Sigma'^i)$ where Σ'^i is a positive diagonal matrix. Then, there exists a scale and permutation matrix $P \in \mathbb{R}^{k \times k}$ such that for all i , $A'^i = A^i P$ and $\Sigma^i = P \Sigma'^i P^T$.*

We propose a likelihood-based approach for learning. As shown in the following derivations, we get a likelihood in closed-form. Let us denote by $W^i = (A^i)^{-1}$ the *unmixing matrices* and view the likelihood as a function of $W^i, \lambda_j^i, \sigma_j$. By integrating over the sources (see also appendix A.1), the negative log-likelihood reads (up to a constant):

$$\begin{aligned} \mathcal{L}(W^i, \lambda_j^i, \sigma_j) &= -\log \left(\int_{\mathbf{s}} p(\mathbf{x}|\mathbf{s}) p(\mathbf{s}) d\mathbf{s} \right) \\ &= \sum_{i=1}^m \left[-\log(|W^i|) + \frac{1}{2} \sum_{j=1}^k \log \left(\frac{(\sigma_j)^2}{(\lambda_j^i)^2 m} \right) \right] - \log(\mathcal{J}) \end{aligned} \quad (2)$$

with

$$\mathcal{J} = \int_{\mathbf{s}} \exp \left(-\sum_{i=1}^m \sum_{j=1}^k \frac{(\lambda_j^i)^2 m}{2(\sigma_j)^2} (y_j^i - s_j)^2 \right) p(\mathbf{s}) d\mathbf{s}$$

where $y_j^i = (W^i \mathbf{x}^i)_j$. This integral is a product of one dimensional integrals since the coefficients of s are independent. We obtain (see appendix A.1):

$$-\log(\mathcal{J}) = \sum_{i,j} \frac{m}{2(\sigma_j)^2} (\lambda_j^i)^2 (y_j^i - \tilde{s}_j)^2 + \sum_j f(\tilde{s}_j, \sigma_j) \text{ where}$$

$$f(\tilde{s}_j, \sigma_j) = -\log \left(\int_z \exp \left(-\frac{m}{2(\sigma_j)^2} z^2 \right) \delta(\tilde{s}_j - z) dz \right)$$

involves the source density δ convolved by a Gaussian kernel and $\tilde{s}_j = \sum_i y_j^i (\lambda_j^i)^2$ is a weighted average of unmixed data.

To make the computation of f available in closed-form while assuming a heavy-tailed distribution, we postulate a particular density δ consisting of the following Gaussian mixture:

$$\delta(s_j) = \frac{1}{2} \left(\mathcal{N}(s_j; 0, \frac{1}{2}) + \frac{1}{2} \mathcal{N}(s_j; 0, \frac{3}{2}) \right). \quad (3)$$

Denoting

$$\phi_j(s_j, \sigma_j) = -\log(\mathcal{N}(s_j; 0, \frac{1}{2} + \frac{\sigma_j^2}{m}) + \mathcal{N}(s_j; 0, \frac{3}{2} + \frac{\sigma_j^2}{m}))$$

$$f \text{ reads: } f(s_j, \sigma_j) = -\frac{1}{2} \log \left(\frac{(\sigma_j)^2}{m} \right) + \phi(s_j, \sigma_j).$$

The negative log-likelihood becomes

$$\begin{aligned} \mathcal{L}(W^i, \lambda_j^i, \sigma_j) &= \sum_{i=1}^m \left[-\log(|W^i|) - \sum_{j=1}^k \frac{1}{2} \log((\lambda_j^i)^2) \right. \\ &\quad \left. + \frac{1}{2} \sum_{j=1}^k \frac{m \lambda_j^{i2}}{(\sigma_j)^2} \left(y_j^i - \sum_{z=1}^m y_j^z (\lambda_j^z)^2 \right)^2 \right] \\ &\quad + \sum_{j=1}^k \left[\frac{1-m}{2} \log \left(\frac{m}{(\sigma_j)^2} \right) + \phi \left(\sum_{z=1}^m y_j^z (\lambda_j^z)^2, \sigma_j \right) \right] \end{aligned} \quad (4)$$

where $\mathbf{y}^i = W^i \mathbf{x}^i$ and $\sum_{i=1}^m (\lambda_j^i)^2 = 1$, for all j . AVICA boils down to minimizing \mathcal{L} . When $\lambda_j^i = \frac{1}{\sqrt{m}}$ and $\sigma_j = 1$ we recover the negative log-likelihood of MultiViewICA Richard et al. (2020). In addition, if we only have one view ($m = 1$), we recover the negative log-likelihood of Infomax Bell & Sejnowski (1995); Cardoso (1997) where the density of the source is replaced by δ convolved with a Gaussian kernel.

The following proposition shows that even if the data do not follow the density δ , there exists a well-defined local minimum where the true unmixing matrices are recovered up to some scaling. We refer to appendix B.2 for the proof.

Proposition 2 (Robustness of AVICA w.r.t. source density misspecification). *Consider \mathbf{x}^i , $i = 1 \dots m$, generated from equation (1) with mixing matrices A^i , relative noise precisions λ_j^{i*} global noise σ_j^* and a source density δ^* not necessarily equal to δ in equation 3.*

We assume the data and the model verify the following hypothesis (H):

$$\exists \mu > 0, \forall i, j \ (\lambda_j^i)^2 \geq \mu^2, \quad (5)$$

There exist scaling matrices Γ^i , relative noise precisions $(\lambda_j^i)_{i=1, j=1}^{m, k}$ and global noise $(\sigma_j)_{j=1}^k$ such that $(\Gamma^i(A^i)^{-1})_{i=1}^m, (\lambda_j^i)_{i=1, j=1}^{m, k}, (\sigma_j)_{j=1}^k$ is a local minimum of \mathcal{L} (4). This minimum is well-defined, meaning it does not occur at the border of the definition set of \mathcal{L} (4).

We include the constraints in (H) in the AVICA model (1) making μ^2 a hyper-parameter fixed to 10^{-3} in all experiments.

2.2 Efficient learning by quasi-Newton MLE

We first propose to optimize \mathcal{L} using an alternating quasi-Newton method we call *quasi-Newton MLE*. Quasi-Newton methods Nocedal & Wright (2006) minimize some function iteratively by following the direction $D = -\tilde{H}^{-1}G$ where \tilde{H}^{-1} is an approximation of the inverse of the Hessian and G is the gradient.

The proposed method is a block coordinate descent approach where we fix all parameters except a specific group that undergoes a quasi-Newton step. We cycle through the groups and repeat the procedure until the gradient norm is below a threshold, indicating that we are close to a stationary point.

Update w.r.t W^i The relative gradient $G^{W^i} \in \mathbb{R}^{k \times k}$ and Hessian $H^{W^i} \in \mathbb{R}^{k, k, k, k}$ satisfy: $\mathcal{L}((I + \epsilon)W^i) = \mathcal{L}(W^i) + \langle \epsilon | G^{W^i} \rangle + \frac{1}{2} \langle \epsilon | H^{W^i} \epsilon \rangle + o(\|\epsilon\|^2)$. The Hessian is given by:

$$H_{abcd}^{W^i} = \delta_{ad}\delta_{bc} + \delta_{ac} \left((\lambda_a^i)^4 \phi''(\tilde{s}_a) + \frac{m}{\sigma_a^2} (1 - (\lambda_a^i)^2)(\lambda_a^i)^2 \right) y_b^i y_d^i$$

for $a, b, c, d = 1 \dots k$, which is expensive to compute. We use a similar approximation as in Ablin et al. (2018), leading to the approximation:

$$\tilde{H}_{abcd}^{W^i} = \delta_{ad}\delta_{bc} + \delta_{ac}\delta_{bd} \left((\lambda_a^i)^4 \phi''(\tilde{s}_a) + \frac{m}{\sigma_a^2} (1 - (\lambda_a^i)^2)(\lambda_a^i)^2 \right) (y_b^i)^2 \quad (6)$$

This approximation is exact when the unmixed data \mathbf{y}^i are independent. Therefore as we get closer to convergence, the quality of the approximation improves. Besides, the Hessian approximation is block-diagonal with blocks of size 2×2 , making it easy to invert and regularize. Regularization is indeed necessary to guarantee positivity of the Hessian and therefore a descent direction. Updates are given by

$$W^i \leftarrow (I - \rho(\tilde{H}^{W^i})^{-1}G^{W^i})W^i \quad (7)$$

where $\rho \in \mathbb{R}$ is the stepsize.

The stepsize is chosen by backtracking line-search: we start with $\rho = 1$ and halve the stepsize until it yields a decrease of the loss.

Update w.r.t $(\lambda_j^i)_{i=1}^m$ The relative noise precisions parameters are subject to the two constraints: $\sum_{i=1}^m (\lambda_j^i)^2 = 1$ and $\forall i \ (\lambda_j^i)^2 \geq \mu^2$. To simplify optimization we make the following change of variable: $(\eta_j^i)^2 + \mu^2 = (\lambda_j^i)^2$ and therefore $\boldsymbol{\eta}_j = (\eta_j^1 \dots \eta_j^m)$ is on the sphere of radius $1 - m\mu^2$. Facing optimization on a manifold, we employ a Riemannian strategy based on projection Absil & Malick (2012).

Updates are given by (see Appendix A.2):

$$\boldsymbol{\eta}_j \leftarrow \frac{\boldsymbol{\eta}_j - \rho(H^{\boldsymbol{\eta}_j})^{-1}G^{\boldsymbol{\eta}_j}}{\|\boldsymbol{\eta}_j - \rho(H^{\boldsymbol{\eta}_j})^{-1}G^{\boldsymbol{\eta}_j}\| \sqrt{1 - m\mu^2}} \quad (8)$$

where ρ is the step-size chosen similarly by backtracking line-search and $G^{\boldsymbol{\eta}_j}$ and $H^{\boldsymbol{\eta}_j}$ are respectively the Riemannian gradient and Hessian with respect to $\boldsymbol{\eta}_j$.

Update w.r.t σ_j As there are no constraints on the scalar σ_j , the Newton updates simply read:

$$\sigma_j \leftarrow \sigma_j - \rho \frac{G^{\sigma_j}}{H^{\sigma_j}} \quad (9)$$

where ρ is the step-size again chosen by backtracking line-search.

We provide the formulas for the gradients and Hessians in appendix A.2.

Algorithm 1 Optimization of AVICA via quasi-Newton MLE

Input Dataset $(\mathbf{x}^i)_{i=1}^m$, initial values for W^i , λ_j^i , σ_j . Tolerance parameter $\varepsilon = 10^{-3}$. Constraint parameter $\mu^2 = 10^{-3}$.

Compute η_j^i from λ_j^i , Set $\text{tol} = \infty$.

while $\text{tol} > \varepsilon$ **do**

$\text{tol} = 0$

for $i = 1 \dots m$ **do**

 Compute $(\tilde{H}^{W^i})^{-1}G^{W^i}$ using the Hessian approximation in equation (6) and update W^i using (7)

 Set $\text{tol} = \max(\text{tol}, \|G^{W^i}\|_\infty)$

end for

for $j = 1 \dots k$ **do**

 Compute $(H^{\eta_j})^{-1}G^{\eta_j}$ and update η_j using (8)

$\text{tol} = \max(\text{tol}, \|G^{\eta_j}\|_\infty)$

 Compute $(H^{\sigma_j})^{-1}G^{\sigma_j}$ and update σ_j using (9)

 Set $\text{tol} = \max(\text{tol}, \|G^{\sigma_j}\|_\infty)$

end for

end while

Compute λ_j^i from η_j^i

Return unmixing matrices $(W^i)_{i=1}^m$, precisions $(\lambda_j^i)_{i=1, j=1}^{m, k}$, global noise levels $(\sigma_j)_{j=1}^m$, sources $(\mathbb{E}[s_j|\mathbf{x}])_{j=1}^m$ using equation (10).

Stopping criterion While performing the alternating quasi-Newton algorithm, we monitor the norm of the gradients $\|G\|_\infty$ and use them to stop the convergence of AVICA.

The pseudo code for the proposed optimization algorithm is provided in Algorithm 1.

2.3 A closed-form minimum mean square error (MMSE) estimator of sources

Let $\hat{\mathbf{s}}$ an estimate of the sources \mathbf{s} from observations \mathbf{x} . A minimum mean square error (MMSE) estimate of \mathbf{s} minimizes $\hat{\mathbf{s}} \rightarrow \mathbb{E}[\|\hat{\mathbf{s}} - \mathbf{s}\|^2]$. It is unique and given by $\hat{\mathbf{s}} = \mathbb{E}[\mathbf{s}|\mathbf{x}]$. We now derive a closed-form solution for $\hat{\mathbf{s}}$.

Following the computations in appendix C we can write:

$$\begin{aligned} p(\mathbf{x}, \mathbf{s}) &= p(\mathbf{x}|\mathbf{s})p(\mathbf{s}) = \prod_{i=1}^m p(\mathbf{x}^i|\mathbf{s})p(\mathbf{s}) \\ &\propto \prod_{i=1}^m \prod_{j=1}^k \exp\left(-\frac{(\lambda_j^i)^2 m}{2(\sigma_j)^2} (y_j^i - s_j)^2\right) \delta(s_j) \\ &\propto \prod_{j=1}^k \exp\left(-\frac{m}{2(\sigma_j)^2} (\tilde{s}_j - s_j)^2\right) \delta(s_j) \end{aligned}$$

where we leave out terms that do not depend on s_j .

Using our Gaussian mixture assumption on the sources we obtain after following the derivations provided in appendix C :

$$p(\mathbf{x}, \mathbf{s}) \propto \prod_{j=1}^k \sum_{\alpha \in \{\frac{1}{2}, \frac{3}{2}\}} \theta_{\alpha, j} \mathcal{N}(s_j; \tilde{\mu}_j, \tilde{\nu}_j)$$

where $\theta_{\alpha, j} = \mathcal{N}\left(\tilde{s}_j; 0, \sqrt{\alpha + \frac{(\sigma_j)^2}{m}}\right)$, $\tilde{\mu}_j = \frac{m\alpha\tilde{s}_j}{m\alpha + (\sigma_j)^2}$ and $\tilde{\nu}_j = \frac{(\sigma_j)^2\alpha}{m\alpha + (\sigma_j)^2}$. Therefore

$$p(\mathbf{s}|\mathbf{x}) = \frac{p(\mathbf{x}, \mathbf{s})}{p(\mathbf{x})} = \prod_{j=1}^k \frac{\sum_{\alpha \in \{\frac{1}{2}, \frac{3}{2}\}} \theta_{\alpha, j} \mathcal{N}(s_j; \tilde{\mu}_j, \tilde{\nu}_j)}{\sum_{\alpha \in \{\frac{1}{2}, \frac{3}{2}\}} \theta_{\alpha, j}}$$

We then obtain a MMSE estimator:

$$\mathbb{E}[s_j|\mathbf{x}] = \frac{\sum_{\alpha \in \{\frac{1}{2}, \frac{3}{2}\}} \theta_{\alpha, j} \tilde{\mu}_j}{\sum_{\alpha \in \{\frac{1}{2}, \frac{3}{2}\}} \theta_{\alpha, j}} \quad (10)$$

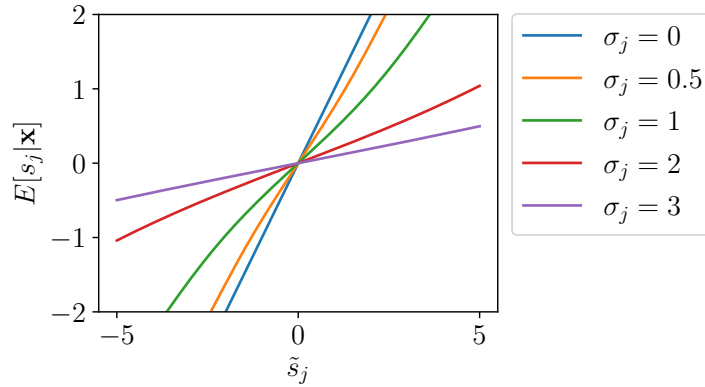


Figure 1: **MMSE estimator**: Plot of the MMSE estimator $\mathbb{E}[s_j|\mathbf{x}]$ in function of \tilde{s}_j and σ_j with $m = 1$.

which is used in the rest of the paper as our estimate of the common sources. The MMSE estimator weights the unmixed data of each view based on the relative noise precisions estimates and then applies a non-linear shrinkage. A plot of $\mathbb{E}[s_j|\mathbf{x}]$ in function of \tilde{s}_j and σ_j with $m = 1$ is given in Figure 1. We see that the shrinkage is stronger for the more noisy sources.

2.4 Quasi-Newton Expectation Maximization algorithm

The second method we propose to maximize the log-likelihood is a generalized EM Neal & Hinton (1998); Dempster et al. (1977), which we call *quasi-Newton EM* as it involves quasi-Newton steps. The closed-form for $p(\mathbf{s}|\mathbf{x})$ makes the implementation of the E-step simple.

The complete negative log-likelihood is given by:

$$\begin{aligned} \mathcal{C} &= -\log\left(\prod_{i=1}^m p(\mathbf{x}^i|\mathbf{s})p(\mathbf{s})\right) \\ &= \sum_{i=1}^m [-\log(|W^i|) - \log(\mathcal{N}(\mathbf{y}^i; \mathbf{s}, \Sigma^i))] + \text{const} \end{aligned}$$

This complete negative log-likelihood is quadratic in \mathbf{s} and therefore we only need $\mathbb{E}[\mathbf{s}|\mathbf{x}]$ given in (10) and $\text{Var}[\mathbf{s}|\mathbf{x}]$ given by

$$\text{Var}[s_j|\mathbf{x}] = \frac{\sum_{\alpha \in \{\frac{1}{2}, \frac{3}{2}\}} \theta_{\alpha,j} \tilde{\nu}_j}{\sum_{\alpha \in \{\frac{1}{2}, \frac{3}{2}\}} \theta_{\alpha,j}}.$$

We then minimize the negative complete log-likelihood with respect to Σ^i and W^i . Computing the gradient with respect to Σ^{i-1} we get the closed-form updates for Σ^i :

$$\Sigma^i \leftarrow \text{diag}(\mathbb{E}[(\mathbf{y}^i - \mathbb{E}[\mathbf{s}|\mathbf{x}])(\mathbf{y}^i - \mathbb{E}[\mathbf{s}|\mathbf{x}])^\top] + \text{Var}[\mathbf{s}|\mathbf{x}])$$

We update W^i by performing a quasi-Newton step. The gradient \mathcal{G}^{W^i} and the Hessian \mathcal{H}^{W^i} are given by

$$\begin{aligned} \mathcal{G}^{W^i} &= -I + (\Sigma^i)^{-1}(\mathbf{y}^i - \mathbb{E}[\mathbf{s}|\mathbf{x}])(\mathbf{y}^i)^\top \\ \mathcal{H}_{a,b,c,d}^{W^i} &= \delta_{a,c} \frac{y_b^i y_d^i}{\Sigma_a^i} \simeq \delta_{a,c} \delta_{b,d} \frac{(y_b^i)^2}{\Sigma_a^i} \end{aligned}$$

where we use a similar Hessian approximation as in equation (6). We give detailed derivations in Appendix D.

Updates for W^i are then given by

$$W^i \leftarrow (I - \rho(\mathcal{H}^{W^i})^{-1}\mathcal{G}^{W^i})W^i,$$

where ρ is chosen by backtracking line-search. We alternate between computing the statistics $\mathbb{E}[\mathbf{s}|\mathbf{x}]$ and $\text{Var}[\mathbf{s}|\mathbf{x}]$ (E-step) and updates of parameters Σ^i and W^i (M-step). We can compute λ_j^i and σ_j from $(\Sigma_j^i)_{i=1}^m$ using

$\sigma_j = \left(\frac{1}{m} \sum_{i=1}^m \frac{1}{\Sigma_j^i}\right)^{-1/2}$ and $(\lambda_j^i)^2 = \frac{(\sigma_j^i)^2}{\Sigma_j^i m}$ and monitor the convergence using the gradients with respect to the actual log-likelihood in equation (4).

3 Related work

A number of methods are available in the literature to perform group ICA.

A popular approach Calhoun et al. (2001) is to concatenate all the views and then apply PCA in order to obtain a reduced representation that has the same number of dimensions as in one view. ICA is then applied on the reduced representation. We refer to this method as *ConcatICA* in the experiments. A related approach called *CanICA* Varoquaux et al. (2009) uses multi-set CCA instead of PCA for fusing the views. Lastly another fast approach is *PermICA* Esposito et al. (2005); Hyvärinen (2011) that estimates the sources from each view separately. The sources are then matched across views using the Hungarian algorithm Tichavsky & Koldovsky (2004) and the matched sources are averaged to yield an estimate for the common sources. These three methods are very fast but they do not optimize a proper likelihood so they do not benefit from the advantages of such estimators such as statistical efficiency.

The tensorial approach of Beckmann & Smith (2005) imposes a particular structure on the unmixing matrices so that unmixing matrices of different views are row-wise scaled version of one another. This approach can model view-specific and source-specific variability via the row-wise scaling but imposes a structure on the unmixing matrices that may be limiting. AVICA does not have such constraints and still enjoys identifiability.

Two extensions of Beckmann & Smith (2005) are presented in Guo & Pagnoni (2008). The first extension is useful when views belong to different groups but it keeps the same constraints on the unmixing matrices. The second extension is more general and relaxes the constraints on the unmixing matrices while allowing for Gaussian additive noise. However the covariance of the additive noise is assumed to be the same for each view.

A more recent approach, MultiViewICA Richard et al. (2020) (*MVICA*) assumes noise on the sources and proposes an efficient likelihood based approach to optimize it. However it assumes a fixed and identical noise variance for all views and sources. In contrast, AVICA infers the noise variance and allows it to differ depending on views and sources. This allows AVICA to weight the estimates of the common sources from each view based on how noisy they are, yielding in the end a better estimate of the shared sources (as will be seen in Figure 3 below).

4 Experiments

4.1 Dimension reduction and initialization

Dimension reduction In this work, the number of sources is assumed to be equal to the number of sensors so that the mixing matrices have square shape. However, in practice the number of sensors can be much larger than the desired number of sources. In the experiments section we use view-specific PCA to perform dimension reduction when using MEG data or when performing spatial ICA on fMRI data. Following the suggestion of Richard et al. (2020) we use the shared response model (SRM, Chen et al. (2015)) to reduce the data dimension when applying temporal ICA on fMRI data. Note that the choice of dimension reduction technique generally has an impact on the results. However we leave this discussion to future work.

Initialization The ICA problem is non convex, therefore the result depends on its initialization. ConcatICA, PermICA and CanICA are randomly initialized. AVICA and MVICA are initialized using ConcatICA.

Software tools Experiments used Nilearn Abraham et al. (2014) and MNE Gramfort et al. (2013) for fMRI and MEG data processing respectively, as well as the scientific Python ecosystem: Matplotlib Hunter (2007), Scikit-learn Pedregosa et al. (2011), Numpy Harris et al. (2020), Scipy Virtanen et al. (2020) and Sympy Meurer et al. (2017).

4.2 Synthetic experiments

We first validate the proposed estimator for the AVICA model using synthetic data generated according to the model in equation (1). The sources are generated i.i.d. from a Laplace density $\delta(x) = \frac{1}{\sqrt{2}} \exp(-\sqrt{2}|x|)$.

Convergence plot We use $m = 10$ views and $k = 5$ sources. Mixing matrices $(A^i)_{i=1}^m$ are generated with i.i.d. entries following a normal distribution. For each source, the relative noise precisions $((\lambda_j^i)^2)_{i=1}^m$ are generated from a Dirichlet distribution with parameter $(1 \dots 1)$. The log of the global noise levels $(\log(\sigma_j))_{j=1}^k$ are generated from a normal distribution where the mean is fixed to 0 and the variance is fixed to $\frac{1}{2}$. We generate $n = 1000$ samples. We set $\mu = 0$ so that the two methods optimize the exact same log-likelihood.

For each optimizer we run the following analysis 100 times with 100 different seeds. At each iteration, we record the ℓ_∞ norm of the gradient with respect to the noise parameters, the ℓ_∞ norm of the gradient with respect to the unmixing matrices, the negative log-likelihood and the current time. We interpolate between time

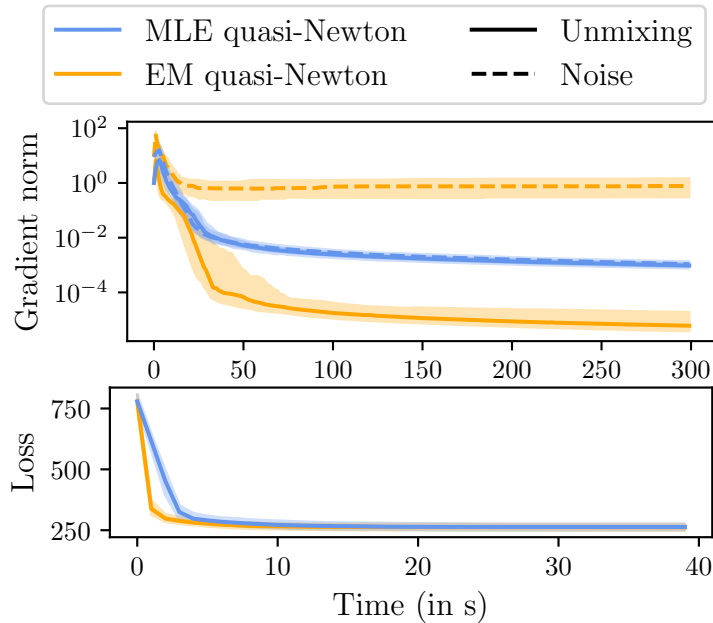


Figure 2: **Synthetic experiment - Convergence plot**: Median gradient norm (top) and negative log-likelihood (bottom) as a function of time. Dashed lines correspond to the gradient with respect to noise parameters and solid lines to the gradient with respect to unmixing matrices. Error bars display the first and last quartiles.

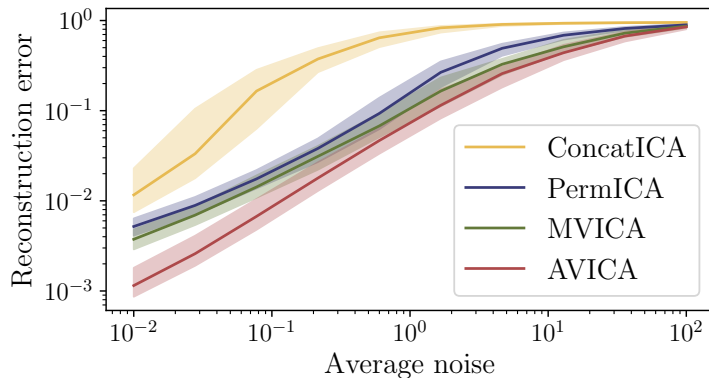


Figure 3: **Synthetic experiment - Reconstruction error**: Median distance between true and recovered sources. Error bars display the first and last quartiles.

points so that we can present convergence curves in function of computation time in Figure 2. We report the median value, and error bars correspond to the first and last quartiles.

The EM quasi-Newton is slightly faster. However the homogeneous decrease of the norm of the different gradients in MLE quasi-Newton makes it easier to monitor. In our experiments we use MLE quasi-Newton as our optimizer. Other convergence plots are available in appendix E.1

Improved reconstruction error of AVICA We use the same generative model as above but the log of the global noise level $(\log(\sigma_j))_{j=1}^k$ are generated from a normal distribution where the mean varies between -2 and 2 (the variance is still fixed to $\frac{1}{2}$). Each compared algorithm returns an estimates of the sources. The performance is measured by computing the reconstruction error which is defined as $1 - \mathbb{E}[\mathbf{s}\hat{\mathbf{s}}]$ where \mathbf{s} are the true sources and $\hat{\mathbf{s}}$ are the estimated sources both normalized so that they have unit variance. Each experiment is repeated 100 times with 100 different seeds. We report the median value, and error bars correspond to the first and last quartiles.

Figure 3 shows that Adaptive multiViewICA outperforms other approaches even though the density used to generate the data is not the same as the one used in the model.

Additional experiments show in appendix E.3 that AVICA recovers well the relative noise precisions parameters and in appendix E.2 that AVICA prioritizes informative views.

4.3 fMRI experiments

fMRI data and preprocessing We use four different fMRI datasets. For each dataset, we specify the number of views m which is the number of subjects and the number of samples n which is the number of brain images per subject. Due to the acquisition pipeline, the samples are generally split into groups of approximately identical size called *runs*. The data have been preprocessed following standard procedures for fMRI data, including realignment within and across runs, and resampling to the template MNI space. Data have been band-pass filtered in the temporal domain in the $[.01, .1]$ Hz range. The *sherlock* dataset Chen et al. (2017) contains $m = 16$ subjects and $n = 1976$ brain images per subject split into 5 runs. The subjects are watching one episode of the “Sherlock” TV show. The *forrest* dataset Hanke et al. (2014) contains $m = 16$ subjects and $n = 3261$ brain images per subject split into 7 runs. The subjects are listening to an audio version of the “Forrest Gump” movie. The *raiders* dataset Pinho et al. (2018) contains $m = 11$ subjects and $n = 3252$ brain images per subject split into 10 runs. The subjects are watching the “Raiders of the Lost ark” movie. The *clips* dataset Pinho et al. (2018) contains $m = 12$ subjects and $n = 3900$ brain images per subject split into 12 runs. The subjects are watching video clips (without audio).

Reconstructing the BOLD signal of missing subjects We reproduce the experimental pipeline of Richard et al. (2020) to benchmark group ICA methods using their ability to reconstruct fMRI data of a left-out subject.

All data undergo a 6 mm spatial smoothing and we focus on the same regions of interests (ROI) as in Richard et al. (2020) that are also reported in Appendix E.4. We call a *forward operator* the product of the dimension reduction operator and an unmixing matrix and a *backward operator* its pseudo inverse. There is one forward operator and one backward operator per view.

The forward operators are learned using all subjects and 80% of the runs. Then they are applied on the remaining 20% of the runs using 80% of the subjects yielding unmixed data. In order to obtain an estimate of the shared sources the unmixed data are averaged. When AVICA is used, this average becomes a weighted average where the weights are given by $(\lambda_j^i)^2$. We then apply the backward operator of the remaining 20% subjects on the shared sources to reconstruct their data.

The accuracy of the reconstruction is measured via the R^2 score which measures for each voxel the discrepancy between the true timecourse \mathbf{z} and the predicted timecourse $\hat{\mathbf{z}}$: $R^2(\hat{\mathbf{z}}, \mathbf{z}) = 1 - \frac{\sum_{t=1}^n (z_t - \hat{z}_t)^2}{\sum_{t=1}^n (z_t - \bar{z})^2}$ where $\bar{z} = \frac{1}{n} \sum_{t=1}^n z_t$ is the empirical mean of \mathbf{z} .

For each compared algorithm, the experiment is run 25 times with different seeds to obtain error bars. We report the mean R^2 score across voxels and display the results in Figure 4. The error bars represent a 95% confidence interval. The chance level is given by the performance of an algorithm that computes its dimension reduction operator and unmixing matrices by sampling from a standard normal distribution.

AVICA exhibits a small improvement on *sherlock* and *raiders* datasets that is consistent for different numbers of components (i.e. numbers of sources) and competitive results on *clips* and *forrest* datasets.

In appendix E.5, an experiment on rest fMRI data shows that AVICA yields more stable sources than other approaches.

4.4 MEG experiments

In the following experiments we consider the Cam-CAN dataset Taylor et al. (2017). We use the magnetometer data from the MEG of $m = 496$ subjects. Each subject is repeatedly presented three audio-visual stimuli. For each stimulus, we divide the trials into two sets and within each set, the MEG signal is averaged across trials to isolate the evoked response. This procedure yields 6 chunks of individual data.

The 6 chunks of data are concatenated in the time direction and ICA algorithms are applied separately to extract $k = 10$ shared sources that we plot in appendix E.7 and localize in appendix E.8.

Robustness w.r.t intra-subject variability in MEG We first study the similarity between group sources corresponding to repetitions of the same stimuli. This gives a measure of robustness of each ICA algorithm with respect to intra-subject variability, or sampling noise.

Algorithms are run 10 times with different seeds on the 6 chunks of data, and group sources are extracted. When two chunks of data correspond to repetitions of the same stimulus they should yield similar sources. For each source and for each stimulus, we therefore measure the ℓ_2 distance between the two repetitions of the stimulus. This yields 300 distances per algorithm that are plotted on Figure 5.

The sources recovered by AVICA have a lower variability than other approaches. The difference between AVICA and other approaches can be quantified via a statistical t-test on the difference of log distances. It gives the p-values 4.57×10^{-4} , 5.93×10^{-4} and 2.37×10^{-9} w.r.t. MVICA, PermICA and ConcatICA respectively.

Recovering the correct noise level in MEG data Here, we study the ability of AVICA to correctly estimate the noise level. For each subject we concatenate the signal corresponding to the 6 chunks of data and

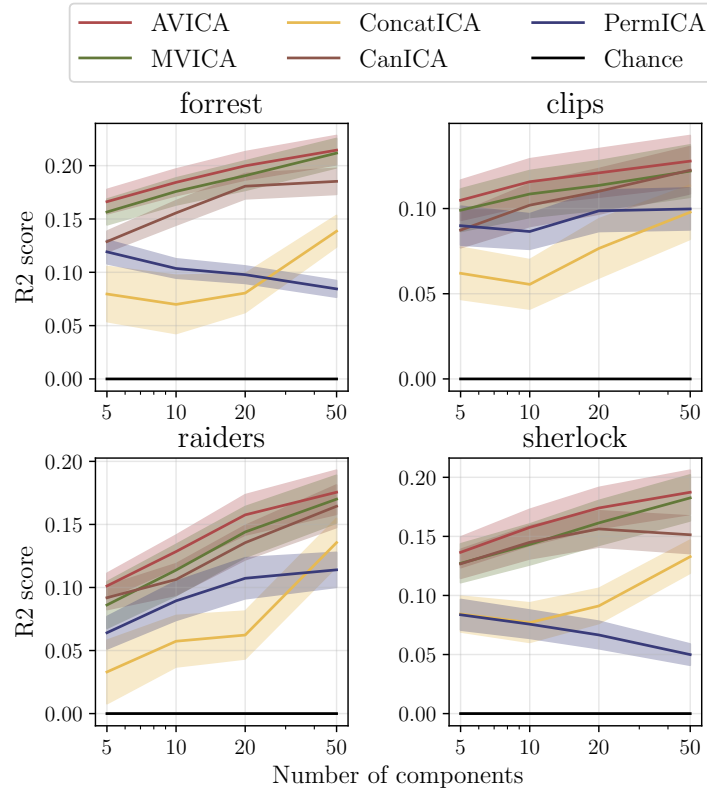


Figure 4: **Reconstructing the BOLD signal of missing subjects.** Mean R^2 score between reconstructed data and true data (higher is better). Error bars represent a 95 % confidence interval.

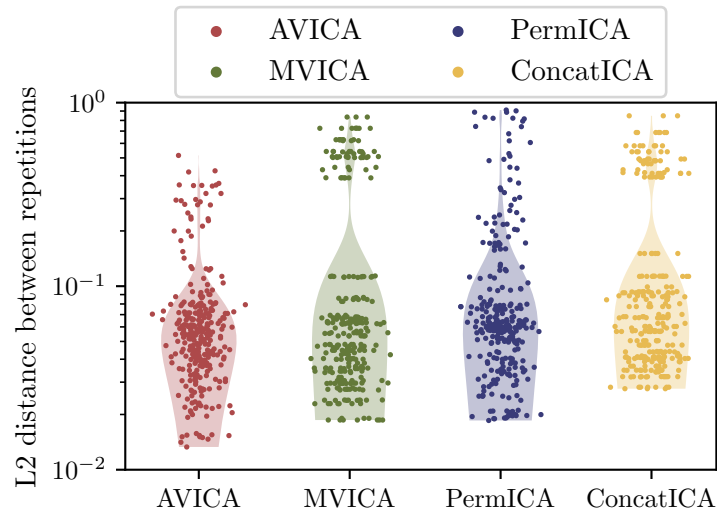


Figure 5: **Robustness w.r.t intra-subject variability in MEG:** Algorithms are run 10 times with different seeds on preprocessed MEG CamCAN data containing 6 chunks of data (2 repetitions for each of the 3 stimulus). We display a scatter plot showing for each algorithm the distance between group sources corresponding to repetitions of the same stimulus.

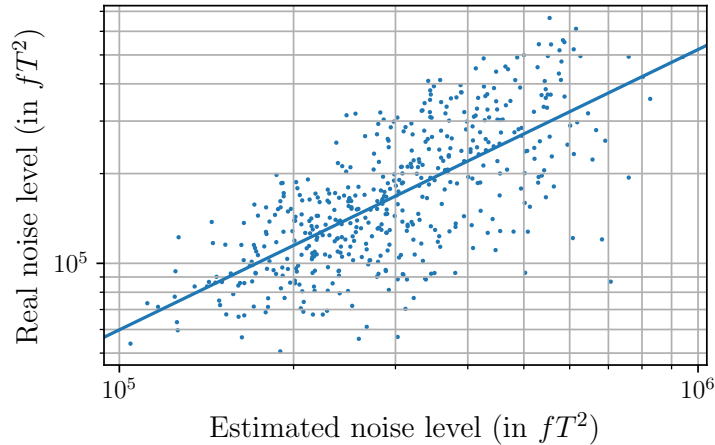


Figure 6: **Estimating noise level in CamCAN MEG:** Scatter plot showing the true noise level and the noise level estimated by Adaptive multiViewICA. We fit a linear regression on the log of the true and predicted noise level: $r^2 = 0.50$ ($p < 10^{-74}$).

compute the mean square error of the baseline (spontaneous) activity - when the subject is not exposed to any stimulus. This quantity is assumed to reflect the true noise level of this subject which we compare to the noise level estimated by AVICA: $\text{tr}(A_i \Sigma_i A_i^\top)$ where $A_i = W_i^{-1}$.

Figure 6 shows a scatter plot that compares the estimated and true noise level. We take the log of the predicted and true noise level and fit a linear regression: we obtain a r^2 score of 0.50 and a p-value of the slope below 10^{-74} .

An additional MEG experiments on phantom data in appendix E.6 demonstrates that AVICA recovers better source estimates than other approaches.

Conclusion

We introduced AVICA, a principled method to solve the group ICA problem, which is an important case of multiview learning. The model explicitly estimates noise levels for each subject and source, which has not hitherto been possible. AVICA enables a closed-form likelihood, which can be minimized quickly with an alternate quasi-Newton method or a generalized EM algorithm. Unlike previous models, AVICA also enables a closed-form MMSE estimator of the sources.

AVICA exhibits performance superior to other group ICA methods on synthetic data and real data involving two different neuroimaging modalities. Experiments on neuroimaging data suggest that AVICA is the method of choice to fuse data across subjects. Future work could investigate whether the common representation learned by AVICA leads to a plausible template of the human brain, as well as the interplay with dimension reduction.

References

- Ablin, P., Cardoso, J.-F., and Gramfort, A. Faster independent component analysis by preconditioning with Hessian approximations. *IEEE Transactions on Signal Processing*, 66(15):4040–4049, 2018.
- Abraham, A., Pedregosa, F., Eickenberg, M., Gervais, P., Mueller, A., Kossaifi, J., Gramfort, A., Thirion, B., and Varoquaux, G. Machine learning for neuroimaging with scikit-learn. *Frontiers in neuroinformatics*, 8:14, 2014.
- Absil, P.-A. and Malick, J. Projection-like retractions on matrix manifolds. *SIAM Journal on Optimization*, 22(1):135–158, 2012.
- Beckmann, C. F. and Smith, S. M. Tensorial extensions of independent component analysis for multisubject fMRI analysis. *Neuroimage*, 25(1):294–311, 2005.
- Bell, A. J. and Sejnowski, T. J. An information-maximization approach to blind separation and blind deconvolution. *Neural computation*, 7(6):1129–1159, 1995.
- Calhoun, V. D., Adali, T., Pearlson, G. D., and Pekar, J. J. A method for making group inferences from functional MRI data using independent component analysis. *Human brain mapping*, 14(3):140–151, 2001.

- Cardoso, J.-F. Infomax and maximum likelihood for blind source separation. *IEEE Signal processing letters*, 4(4):112–114, 1997.
- Chen, J., Leong, Y. C., Honey, C. J., Yong, C. H., Norman, K. A., and Hasson, U. Shared memories reveal shared structure in neural activity across individuals. *Nature neuroscience*, 20(1):115–125, 2017.
- Chen, P.-H., Chen, J., Yeshurun, Y., Hasson, U., Haxby, J., and Ramadge, P. J. A reduced-dimension fMRI shared response model. In *Advances in Neural Information Processing Systems*, pp. 460–468, 2015.
- Chen, Y., Härdle, W., and Spokoiny, V. Portfolio value at risk based on independent component analysis. *Journal of Computational and Applied Mathematics*, 205(1):594–607, 2007.
- Comon, P. Independent component analysis, a new concept? *Signal processing*, 36(3):287–314, 1994.
- Dempster, A. P., Laird, N. M., and Rubin, D. B. Maximum likelihood from incomplete data via the em algorithm. *Journal of the Royal Statistical Society: Series B (Methodological)*, 39(1):1–22, 1977.
- Esposito, F., Scarabino, T., Hyvärinen, A., Himberg, J., Formisano, E., Comani, S., Tedeschi, G., Goebel, R., Seifritz, E., and Salle, F. D. Independent component analysis of fMRI group studies by self-organizing clustering. *NeuroImage*, 25(1):193–205, 2005.
- Gramfort, A., Luessi, M., Larson, E., Engemann, D. A., Strohmeier, D., Brodbeck, C., Goj, R., Jas, M., Brooks, T., Parkkonen, L., et al. MEG and EEG data analysis with MNE-Python. *Frontiers in neuroscience*, 7:267, 2013.
- Guo, Y. and Pagnoni, G. A unified framework for group independent component analysis for multi-subject fMRI data. *NeuroImage*, 42(3):1078–1093, 2008.
- Hanke, M., Baumgartner, F. J., Ibe, P., Kaule, F. R., Pollmann, S., Speck, O., Zinke, W., and Stadler, J. A high-resolution 7-Tesla fMRI dataset from complex natural stimulation with an audio movie. *Scientific data*, 1:140003, 2014.
- Harris, C. R., Millman, K. J., van der Walt, S. J., Gommers, R., Virtanen, P., Cournapeau, D., Wieser, E., Taylor, J., Berg, S., Smith, N. J., Kern, R., Picus, M., Hoyer, S., van Kerkwijk, M. H., Brett, M., Haldane, A., del Río, J. F., Wiebe, M., Peterson, P., G’erard-Marchant, P., Sheppard, K., Reddy, T., Weckesser, W., Abbasi, H., Gohlke, C., and Oliphant, T. E. Array programming with NumPy. *Nature*, 585(7825):357–362, September 2020. doi: 10.1038/s41586-020-2649-2. URL <https://doi.org/10.1038/s41586-020-2649-2>.
- Hunter, J. D. Matplotlib: A 2d graphics environment. *Computing in science & engineering*, 9(3):90–95, 2007.
- Hyvärinen, A. Independent component analysis in the presence of gaussian noise by maximizing joint likelihood. *Neurocomputing*, 22(1-3):49–67, 1998.
- Hyvärinen, A. Testing the ICA mixing matrix based on inter-subject or inter-session consistency. *NeuroImage*, 58(1):122–136, 2011.
- Hyvärinen, A. and Oja, E. Independent component analysis: algorithms and applications. *Neural networks*, 13(4-5):411–430, 2000.
- Liebermeister, W. Linear modes of gene expression determined by independent component analysis. *Bioinformatics*, 18(1):51–60, 2002.
- Liu, T. T. Noise contributions to the fmri signal: An overview. *NeuroImage*, 143:141–151, 2016.
- Maino, D., Farusi, A., Baccigalupi, C., Perrotta, F., Banday, A., Bedini, L., Burigana, C., De Zotti, G., Górski, K., and Salerno, E. All-sky astrophysical component separation with fast independent component analysis (fastica). *Monthly Notices of the Royal Astronomical Society*, 334(1):53–68, 2002.
- Meurer, A., Smith, C. P., Paprocki, M., Čertík, O., Kirpichev, S. B., Rocklin, M., Kumar, A., Ivanov, S., Moore, J. K., Singh, S., Rathnayake, T., Vig, S., Granger, B. E., Muller, R. P., Bonazzi, F., Gupta, H., Vats, S., Johansson, F., Pedregosa, F., Curry, M. J., Terrel, A. R., Roučka, v., Saboo, A., Fernando, I., Kulal, S., Cimrman, R., and Scopatz, A. Sympy: symbolic computing in python. *PeerJ Computer Science*, 3:e103, January 2017. ISSN 2376-5992. doi: 10.7717/peerj-cs.103. URL <https://doi.org/10.7717/peerj-cs.103>.
- Neal, R. M. and Hinton, G. E. A view of the em algorithm that justifies incremental, sparse, and other variants. In *Learning in graphical models*, pp. 355–368. Springer, 1998.
- Nocedal, J. and Wright, S. *Numerical optimization*. Springer Science & Business Media, 2006.

- Pascual-Marqui, R. D. et al. Standardized low-resolution brain electromagnetic tomography (sLORETA): technical details. *Methods Find Exp Clin Pharmacol*, 24(Suppl D):5–12, 2002.
- Pedregosa, F., Varoquaux, G., Gramfort, A., Michel, V., Thirion, B., Grisel, O., Blondel, M., Prettenhofer, P., Weiss, R., Dubourg, V., et al. Scikit-learn: Machine learning in Python. *the Journal of machine Learning research*, 12:2825–2830, 2011.
- Penny, W. and Holmes, A. Random effects analysis. *Statistical parametric mapping: The analysis of functional brain images*, 156:165, 2007.
- Pinho, A. L., Amadon, A., Ruest, T., Fabre, M., Dohmatob, E., Denghien, I., Ginisty, C., Becuwe-Desmidt, S., Roger, S., Laurier, L., et al. Individual brain charting, a high-resolution fMRI dataset for cognitive mapping. *Scientific data*, 5, 2018.
- Richard, H., Gresele, L., Hyvarinen, A., Thirion, B., Gramfort, A., and Ablin, P. Modeling shared responses in neuroimaging studies through multiview ica. In *Advances in Neural Information Processing Systems 33*, December 2020.
- Ristaniemi, T. On the performance of blind source separation in cdma downlink. In *Proceedings of the International Workshop on Independent Component Analysis and Signal Separation (ICA '99)*, pp. 437–441, 1999.
- Taylor, J. R., Williams, N., Cusack, R., Auer, T., Shafto, M. A., Dixon, M., Tyler, L. K., Henson, R. N., et al. The Cambridge Centre for Ageing and Neuroscience (Cam-CAN) data repository: structural and functional MRI, MEG, and cognitive data from a cross-sectional adult lifespan sample. *Neuroimage*, 144:262–269, 2017.
- Tichavsky, P. and Koldovsky, Z. Optimal pairing of signal components separated by blind techniques. *IEEE Signal Processing Letters*, 11(2):119–122, 2004.
- Van Essen, D. C., Smith, S. M., Barch, D. M., Behrens, T. E., Yacoub, E., Ugurbil, K., Consortium, W.-M. H., et al. The WU-Minn human connectome project: an overview. *Neuroimage*, 80:62–79, 2013.
- Varoquaux, G., Sadaghiani, S., Poline, J.-B., and Thirion, B. CanICA: Model-based extraction of reproducible group-level ica patterns from fMRI time series. *arXiv preprint arXiv:0911.4650*, 2009.
- Virtanen, P., Gommers, R., Oliphant, T. E., Haberland, M., Reddy, T., Cournapeau, D., Burovski, E., Peterson, P., Weckesser, W., Bright, J., van der Walt, S. J., Brett, M., Wilson, J., Millman, K. J., Mayorov, N., Nelson, A. R. J., Jones, E., Kern, R., Larson, E., Carey, C. J., Polat, İ., Feng, Y., Moore, E. W., VanderPlas, J., Laxalde, D., Perktold, J., Cimrman, R., Henriksen, I., Quintero, E. A., Harris, C. R., Archibald, A. M., Ribeiro, A. H., Pedregosa, F., van Mulbregt, P., and SciPy 1.0 Contributors. SciPy 1.0: Fundamental Algorithms for Scientific Computing in Python. *Nature Methods*, 17:261–272, 2020. doi: 10.1038/s41592-019-0686-2.

A Likelihood

A.1 The closed-form likelihood of AVICA

Here show the full derivation for likelihood computation

$$\mathcal{L} = -\log \left(\int_{\mathbf{s}} p(\mathbf{x}|\mathbf{s})p(\mathbf{s})d\mathbf{s} \right) \quad (11)$$

$$= -\log \left(\int_{\mathbf{s}} \prod_i p(\mathbf{x}^i|\mathbf{s})p(\mathbf{s})d\mathbf{s} \right) \quad (12)$$

$$= -\log \left(\int_{\mathbf{s}} \prod_i \left[|W^i| \frac{\exp(-\sum_{j=1}^k \frac{m(\lambda_j^i)^2}{2(\sigma_j)^2} (y_j^i - s_j)^2)}{\prod_{j=1}^k \sqrt{2\pi \frac{(\sigma_j)^2}{m(\lambda_j^i)^2}}} \right] p(\mathbf{s})d\mathbf{s} \right) \quad (13)$$

$$= \sum_{i=1}^m \left[-\log(|W^i|) + \frac{1}{2} \sum_{j=1}^k \log \left(\frac{(\sigma_j)^2}{(\lambda_j^i)^2 m} \right) \right] - \log(\mathcal{J}) + \text{const} \quad (14)$$

with

$$\mathcal{J} = \int_{\mathbf{s}} \exp \left(-\sum_{i=1}^m \sum_{j=1}^k \frac{(\lambda_j^i)^2 m}{2(\sigma_j)^2} (y_j^i - s_j)^2 \right) p(\mathbf{s})d\mathbf{s}$$

In (12) we use the conditional independence of \mathbf{x}^i given \mathbf{s} , in (13) we make the change of variable $\mathbf{n}^i = \mathbf{y}^i - \mathbf{s}$ where $\mathbf{y}^i = W^i \mathbf{x}^i$ and use the Gaussian assumption on \mathbf{n}^i . We obtain (14) which is identical to (2) up to a constant.

We then write:

$$\mathcal{J} = \int_{\mathbf{s}} \exp \left(-\sum_{i=1}^m \sum_{j=1}^k \frac{(\lambda_j^i)^2 m}{2(\sigma_j)^2} (y_j^i - s_j)^2 \right) p(\mathbf{s})d\mathbf{s} \quad (15)$$

$$= \int_{\mathbf{s}} \prod_{i=1}^m \prod_{j=1}^k \exp \left(-\frac{(\lambda_j^i)^2 m}{2(\sigma_j)^2} (y_j^i - s_j)^2 \right) \prod_{j=1}^k \delta(s_j) d\mathbf{s} \quad (16)$$

$$= \prod_{j=1}^k \left[\int_{s_j} \exp \left(-\sum_i \frac{(\lambda_j^i)^2 m}{2(\sigma_j)^2} (y_j^i - s_j)^2 \right) \delta(s_j) ds_j \right], \quad (17)$$

where $y_j^i = (\mathbf{w}_j^i)^\top \mathbf{x}^i$. We denote $\tilde{s}_j = \sum_{i=1}^m (\lambda_j^i)^2 y_j^i$. Fix j , and drop it to simplify notation. Then we need to solve the integral

$$\int_s \exp \left(-\sum_i \frac{\lambda_i^2 m}{2\sigma^2} (y^i - s)^2 \right) \delta(s) ds \quad (18)$$

$$= \int_s \exp \left(-\frac{m}{2\sigma^2} \sum_i \lambda_i^2 (y^i - \tilde{s} + \tilde{s} - s)^2 \right) \delta(s) ds \quad (19)$$

$$= \int_s \exp \left(-\frac{m}{2\sigma^2} \sum_i \lambda_i^2 ((y^i - \tilde{s})^2 + (\tilde{s} - s)^2) \right) \delta(s) ds \quad (20)$$

$$= \exp \left(-\frac{m}{2\sigma^2} \sum_i \lambda_i^2 ((y^i - \tilde{s})^2) \right) \int_z \exp \left(-\frac{m}{2\sigma^2} z^2 \right) \delta(\tilde{s} - z) dz \quad (21)$$

where in 21, we make the change of variable $z = \tilde{s} - s$. The remaining integral simply means that δ is smoothed by a Gaussian kernel. We then define $f(s_j, \sigma_j) = -\log \left(\int_z \exp \left(-\frac{m}{2(\sigma_j)^2} z^2 \right) \delta(s_j - z) dz \right)$ and obtain:

$$-\log(\mathcal{J}) = \sum_{i,j} \frac{m}{2(\sigma_j)^2} (\lambda_j^i)^2 (y_j^i - \tilde{s}_j)^2 + \sum_j f(\tilde{s}_j, \sigma_j) \quad (22)$$

A.2 Updates and formulas for gradients and Hessians of loss (4)

Updates w.r.t. λ_j^i Following Absil & Malick (2012), we use the retraction

$$R(\mathbf{x}) = \frac{\mathbf{x}}{\|\mathbf{x}\|\sqrt{1-m\mu^2}} \quad (23)$$

The Riemannian gradient $G^{\boldsymbol{\eta}_j}$ and Hessian $H^{\boldsymbol{\eta}_j}$ of \mathcal{L} are defined by: $\mathcal{L}(\frac{\boldsymbol{\eta}_j + \epsilon}{\|\boldsymbol{\eta}_j + \epsilon\|\sqrt{1-m\mu^2}}) = \mathcal{L}(\boldsymbol{\eta}_j) + \langle \epsilon, G^{\boldsymbol{\eta}_j} \rangle + \frac{1}{2}\langle \epsilon | H^{\boldsymbol{\eta}_j} \epsilon \rangle + o(\|\epsilon\|^2)$ where $\|\boldsymbol{\eta}_j\| = \sqrt{1-m\mu^2}$. Due to the above definitions we get after standard derivations the following relationship between the Riemannian gradient $G^{\boldsymbol{\eta}_j}$ and the Euclidean gradient $\mathbf{g}^{\boldsymbol{\eta}_j}$:

$$G^{\boldsymbol{\eta}_j} = \mathbf{g}^{\boldsymbol{\eta}_j} - \frac{\boldsymbol{\eta}_j}{\|\boldsymbol{\eta}_j\|} \langle \frac{\boldsymbol{\eta}_j}{\|\boldsymbol{\eta}_j\|} | \mathbf{g}^{\boldsymbol{\eta}_j} \rangle \quad (24)$$

The relationship between the Riemannian Hessian $H^{\boldsymbol{\eta}_j}$ and the Euclidean Hessian $\mathcal{H}^{\boldsymbol{\eta}_j}$ is given by:

$$\begin{aligned} H^{\boldsymbol{\eta}_j} = & -\langle G^{\boldsymbol{\eta}_j} | \frac{\boldsymbol{\eta}_j}{\|\boldsymbol{\eta}_j\|^2} \rangle I_m - G^{\boldsymbol{\eta}_j} \left(\frac{\boldsymbol{\eta}_j}{\|\boldsymbol{\eta}_j\|^2} \right)^\top + 3\langle G^{\boldsymbol{\eta}_j} | \frac{\boldsymbol{\eta}_j}{\|\boldsymbol{\eta}_j\|^2} \rangle \boldsymbol{\eta}_j \left(\frac{\boldsymbol{\eta}_j}{\|\boldsymbol{\eta}_j\|^2} \right)^\top \\ & + \left[I_m - \boldsymbol{\eta}_j \left(\frac{\boldsymbol{\eta}_j}{\|\boldsymbol{\eta}_j\|^2} \right)^\top \right] \mathcal{H}^{\boldsymbol{\eta}_j} \left[I_m - \boldsymbol{\eta}_j \left(\frac{\boldsymbol{\eta}_j}{\|\boldsymbol{\eta}_j\|^2} \right)^\top \right] \end{aligned} \quad (25)$$

The gradient $G^{\boldsymbol{\eta}_j}$ and $H^{\boldsymbol{\eta}_j}$ are therefore available in closed-form and updates are given by

$$\boldsymbol{\eta}_j \leftarrow R(\boldsymbol{\eta}_j - \rho(H^{\boldsymbol{\eta}_j})^{-1}G^{\boldsymbol{\eta}_j}) \quad (26)$$

which are the same updates as in (8).

Formulas for gradients and Hessians

- Formulas for W^i : the gradient G^{W^i} is given by

$$G^{W^i} = [(\boldsymbol{\lambda}^i)^2 \odot \phi'(\tilde{\mathbf{s}}, \sigma_j)] (\mathbf{y}^i)^\top + m [\boldsymbol{\sigma}^{-2} \odot (\mathbf{1} - (\boldsymbol{\lambda}^i)^2) \odot (\boldsymbol{\lambda}^i)^2 \odot (\mathbf{y}^i - (\tilde{\mathbf{s}}^{-i}) \odot (\mathbf{1} - (\boldsymbol{\lambda}^i)^2))] (\mathbf{y}^i)^\top - I_k \quad (27)$$

where \odot is the component-wise product and $\boldsymbol{\lambda}^i, \boldsymbol{\sigma}, \mathbf{1} \in \mathbb{R}^k$ are such that $\boldsymbol{\lambda}^i[j] = \lambda_j^i$, $\boldsymbol{\sigma}[j] = \sigma_j^2$ and $\mathbf{1}[j] = 1$ and $\tilde{\mathbf{s}}^{-i} = \sum_{z \neq i} (\boldsymbol{\lambda}^z)^2 \odot \mathbf{y}^z$. The Hessian is given in the main text.

- Formulas for η_j : We give here the Euclidean gradient $\mathbf{g}^{\boldsymbol{\eta}_j}$ and Hessian $\mathcal{H}^{\boldsymbol{\eta}_j}$.

$$\mathbf{g}^{\boldsymbol{\eta}_j} = -\boldsymbol{\eta}_j \odot (\boldsymbol{\lambda}_j)^{-2} + \frac{m}{(\sigma_j)^2} \boldsymbol{\eta}_j \odot (\tilde{\mathbf{s}}_j \mathbf{1} - \mathbf{y}_j)^2 + 2\boldsymbol{\eta}_j \odot \mathbf{y}_j \phi'(\tilde{\mathbf{s}}_j, \sigma_j) \quad (28)$$

$$\begin{aligned} \mathcal{H}^{\boldsymbol{\eta}_j} = & 8 \frac{m}{2\sigma_j^2} (\boldsymbol{\eta}_j \odot (\tilde{\mathbf{s}}_j \mathbf{1} - \mathbf{y}_j)) (\mathbf{y}_j \odot \boldsymbol{\eta}_j)^\top + 8 \frac{m}{2\sigma_j^2} (\mathbf{y}_j \odot \boldsymbol{\eta}_j) (\boldsymbol{\eta}_j \odot (\tilde{\mathbf{s}}_j \mathbf{1} - \mathbf{y}_j))^\top \\ & + 8 (\mathbf{y}_j \odot \boldsymbol{\eta}_j) (\mathbf{y}_j \odot \boldsymbol{\eta}_j)^\top \left(\frac{m}{2\sigma_j^2} + \frac{1}{2} \phi''(\tilde{\mathbf{s}}_j, \sigma_j) \right) \\ & + \text{diag} \left[2\boldsymbol{\eta}_j^2 \odot \boldsymbol{\lambda}_j^{-4} + 2\mathbf{y}_j \phi'(\tilde{\mathbf{s}}_j, \sigma_j) - \frac{1}{\boldsymbol{\lambda}_j^2} + 2 \frac{m}{2\sigma_j^2} (\tilde{\mathbf{s}}_j \mathbf{1} - \mathbf{y}_j)^2 \right] \end{aligned}$$

- Formulas for σ_j : the gradient G^{σ_j} and Hessian H^{σ_j} are given by

$$G^{\sigma_j} = \frac{(m-1)}{\sigma_j} - \frac{m}{\sigma_j^3} \left(\sum_i (\lambda_j^i)^2 (y_j^i - \tilde{s}_j)^2 \right) + \frac{\partial \phi}{\partial \sigma_j}(\tilde{\mathbf{s}}_j, \sigma_j) \quad (29)$$

$$H^{\sigma_j} = -\frac{(m-1)}{\sigma_j^2} + 3 \frac{m}{\sigma_j^4} \left(\sum_i (\lambda_j^i)^2 (y_j^i - \tilde{s}_j)^2 \right) + \frac{\partial \phi}{\partial \sigma_j^2}(\tilde{\mathbf{s}}_j, \sigma_j) \quad (30)$$

B Proofs

B.1 Proof of Proposition 1

We fix a subject i . Since \mathbf{s} has independent non-Gaussian components, it is also the case for $\mathbf{s} + \mathbf{n}^i$. Following Comon (1994), Theorem 11, there exists a scale-permutation matrix P^i such that $A^{i'} = A^i P^i$. As a consequence, we have $\mathbf{s} + \mathbf{n}^i = P^i(\mathbf{s}' + \mathbf{n}'^i)$ for all i . Then, we focus on subject 1 and subject $i \neq 1$:

$$\mathbf{s} + \mathbf{n}^1 - (\mathbf{s} + \mathbf{n}^i) = P^1(\mathbf{s}' + \mathbf{n}'^1) - P^i(\mathbf{s}' + \mathbf{n}'^i) \quad (31)$$

$$\mathbf{n}^1 - \mathbf{n}^i = P^1(\mathbf{s}' + \mathbf{n}'^1) - P^i(\mathbf{s}' + \mathbf{n}'^i) \quad (32)$$

$$\iff P^1 \mathbf{s}' - P^i \mathbf{s}' = P^i \mathbf{n}'^i - \mathbf{n}^i + \mathbf{n}^1 - P^1 \mathbf{n}'^1 \quad (33)$$

This shows that $P^1 \mathbf{s}' - P^i \mathbf{s}'$ is either zero or Gaussian which can only happen if $P^1 = P^i$ (following Lemma 9 of Comon (1994)). Therefore, the matrices P^i are all equal, and there exists a scale and permutation matrix P such that $A^{i'} = A^i P$.

Now we also have

$$\mathbf{s} + \mathbf{n}^i = P(\mathbf{s}' + \mathbf{n}'^i) \quad (34)$$

$$\iff \mathbf{s} - P\mathbf{s}' = P\mathbf{n}'^i - \mathbf{n}^i \quad (35)$$

By a similar argument as before we get $\mathbf{s} = P\mathbf{s}'$ and $\mathbf{n}^i = P\mathbf{n}'^i$ and therefore $\Sigma^i = P\Sigma^{i'}P^\top$.

B.2 Proof of Proposition 2

We denote $W^{i*} = \Gamma^i(A^i)^{-1}$, $(\mathbf{y}^i)^* = W^{i*} \mathbf{x}^i = \Gamma^i(\mathbf{s}^{i*} + \mathbf{n}^{i*})$ and introduce γ_j^i such that $\Gamma^i = \text{diag}(\gamma_1^i \dots \gamma_k^i)$.

The model of AVICA becomes:

$$\begin{aligned} y_j^i &= \frac{1}{\gamma_j^i}(s_j + n_j^i), \quad i = 1, \dots, m \\ p(\mathbf{s}_j) &= \delta(s_j) \\ n_j^i &\sim \mathcal{N}(0, \sigma_j^{i2}) \end{aligned} \quad (36)$$

where $\sigma_j^{i2} = \frac{(\sigma_j)^2}{m(\lambda_j^i)^2}$ and λ_j^i respects the constraints introduced in (\mathcal{H}) and $\sum_{i=1}^m (\lambda_j^i)^2 = 1$ for all j .

Note that there are no interactions between components so the derivations can be performed with only one component (which we omit in the notations for simplicity):

$$p((y^1)^* \dots (y^m)^*) = \int_s \prod_{i=1}^m p((y^i)^* | s) \delta(s) ds \quad (37)$$

$$\leq \int_s p((y^i)^* | s) \delta(s) ds \quad (38)$$

$$= |\gamma^i| \int_s \mathcal{N}(s; \gamma^i (y^i)^*, \sigma^i) \delta(s) ds \quad (39)$$

$$= |\gamma^i| \int_s \frac{\exp(-\frac{(\gamma^i (y^i)^* - s)^2}{2\sigma^{i2}})}{\sqrt{2\pi\sigma^{i2}}} \delta(s) ds \quad (40)$$

From equation 40 we use $\exp(-\frac{(\gamma^i (y^i)^* - s)^2}{2\sigma^{i2}}) \leq 1$ which gives $p(y^{1*} \dots y^{m*}) \leq \frac{|\gamma^i|}{\sqrt{2\pi|\sigma^i|}}$ and therefore denoting $\mathcal{L} = -\log(p(y^{1*} \dots y^{m*}))$ the negative log-likelihood, we have

$$\lim_{\frac{|\gamma^i|}{|\sigma^i|} \rightarrow 0} \mathcal{L} = +\infty \quad (41)$$

for all i .

From equation 39 we use $\mathcal{N}(s; \gamma^i (y^i)^*, \sigma^i) \leq 1$ which gives $p((y^1)^* \dots y^{m*}) \leq |\gamma^i|$ and therefore

$$\lim_{|\gamma^i| \rightarrow 0} \mathcal{L} = +\infty \quad (42)$$

for all i .

We also have

$$p((y^1)^* \cdots (y^m)^*) \quad (43)$$

$$= \int_s \prod_{i=1}^m p((y^i)^* | s) \delta(s) ds \quad (44)$$

$$= \int_s \prod_{i=1}^m \left[|\gamma^i| \int_s \frac{\exp(-\frac{(\gamma^i(y^i)^* - s)^2}{2\sigma^2})}{\sqrt{2\pi\sigma^2}} \delta(s) \right] ds \quad (45)$$

$$= \int_s \prod_{i=1}^m |\gamma^i| \int_s \frac{\exp(-\frac{\sum_i m(\lambda^i)^2 (\gamma^i(y^i)^* - s)^2}{2\sigma^2})}{\sqrt{2\pi \frac{(\sigma^2)^2}{m(\lambda^i)^2}}} \delta(s) ds \quad (46)$$

$$\propto \int_s \prod_{i=1}^m \left[\sqrt{\frac{(\gamma^i)^2 m (\lambda^i)^2}{\sigma^2}} \int_s \exp(-\frac{m}{2\sigma^2} \sum_i [(\lambda^i)^2 (\gamma^i(y^i)^* - s)^2]) \delta(s) ds \right] \quad (47)$$

$$= \int_s \prod_{i=1}^m \left[\sqrt{\frac{(\gamma^i)^2 m (\lambda^i)^2}{\sigma^2}} \int_s \exp(-\frac{m}{2\sigma^2} \sum_i [(\lambda^i)^2 ((\gamma^i(y^i)^* - \tilde{s}^*)^2 + (\tilde{s}^* - s)^2)]) \delta(s) ds \right] \quad (48)$$

$$= \int_s \prod_{i=1}^m \left[\sqrt{\frac{(\gamma^i)^2 m (\lambda^i)^2}{\sigma^2}} \int_s \exp(-\frac{m}{2\sigma^2} \sum_i [(\lambda^i)^2 (\gamma^i(y^i)^* - \tilde{s}^*)^2]) \exp(-\frac{m}{2\sigma^2} (\tilde{s}^* - s)^2) \delta(s) ds \right] \quad (49)$$

$$\leq \prod_{i=1}^m \left[\sqrt{\frac{(\gamma^i)^2 m (\lambda^i)^2}{\sigma^2}} \exp(-\frac{m}{2\sigma^2} \sum_i [(\lambda^i)^2 (\gamma^i(y^i)^* - \tilde{s}^*)^2]) \right] \quad (50)$$

$$= \prod_{i=1}^m \left[\sqrt{\frac{(\gamma^i)^2 m (\lambda^i)^2}{\sigma^2}} \exp(-\frac{m}{2\sigma^2} (\lambda^i)^2 (\gamma^i(y^i)^* - \tilde{s}^*)^2) \right] \quad (51)$$

where in equation 47, we use the parametrization $\sigma^2 = \frac{(\sigma^2)^2}{m(\lambda^i)^2}$ where $\sum_i (\lambda^i)^2 = 1$ and use $\tilde{s}^* = \sum_i (\lambda^i)^2 \gamma^i (y^i)^*$.

In equation 50, we used $\exp(-\frac{m}{2\sigma^2} (\tilde{s}^* - s)^2) \leq 1$.

The negative log-likelihood therefore verifies:

$$\mathcal{L} \geq \sum_{i=1}^m \left[-\frac{1}{2} \log\left(\frac{(\gamma^i)^2 m (\lambda^i)^2}{\sigma^2}\right) + \frac{m}{2\sigma^2} (\lambda^i)^2 (\gamma^i(y^i)^* - \tilde{s}^*)^2 \right] \quad (52)$$

Let us focus on the term $(\gamma^i(y^i)^* - \tilde{s}^*)^2$:

$$(\gamma^i(y^i)^* - \tilde{s}^*)^2 = \left(\gamma^i(s^* + n^{i*}) - \sum_{z=1}^m \gamma^z(s^* + n^{z*}) \lambda^{z2} \right)^2 \quad (53)$$

$$= \left(\gamma^i - \sum_{z=1}^m \gamma^z (\lambda^z)^2 \right)^2 s^{*2} + \left(\gamma^i n^{i*} - \sum_{z=1}^m \gamma^z (\lambda^z)^2 n^{z*} \right)^2 \quad (54)$$

$$\geq \left(\gamma^i n^{i*} - \sum_{z=1}^m \gamma^z (\lambda^z)^2 n^{z*} \right)^2 \quad (55)$$

$$= \left(\gamma^i (1 - (\lambda^i)^2) n^{i*} - \sum_{z=1, z \neq i}^m \gamma^z (\lambda^z)^2 n^{z*} \right)^2 \quad (56)$$

$$\geq (\gamma^i (1 - (\lambda^i)^2) n^{i*})^2 \geq (\gamma^i)^2 c^i \quad (57)$$

where $c^i > 0$ is a strictly positive constant because of (\mathcal{H}) .

Therefore

$$\mathcal{L} \geq \sum_{i=1}^m \left[-\frac{1}{2} \log\left(\frac{(\gamma^i)^2 m (\lambda^i)^2}{\sigma^2}\right) + \frac{m}{2\sigma^2} (\lambda^i)^2 (\gamma^i)^2 c^i \right] \quad (58)$$

$$= \sum_{i=1}^m \left[-\frac{1}{2} \log\left(\frac{(\gamma^i)^2}{(\sigma^i)^2}\right) + \frac{(\gamma^i)^2}{2(\sigma^i)^2} c^i \right] \quad (59)$$

We then have

$$\lim_{\substack{|\gamma^i| \\ |\sigma^i|} \rightarrow \infty} \mathcal{L} = +\infty \quad (60)$$

for all i .

Using (60) and (42) yields

$$\lim_{|\sigma^i| \rightarrow 0} \mathcal{L} = +\infty \quad (61)$$

for all i .

We now study what happens when $\forall i, \gamma^i \rightarrow \infty$ while $\forall i, r^i = \frac{|\sigma^i|}{|\gamma^i|}$ is bounded.

The model becomes

$$\begin{aligned} y^i &= a^i s + n^i, \quad i = 1, \dots, m \\ p(s) &= \delta(s) \\ n^i &\sim \mathcal{N}(0, (r^i)^2) \end{aligned}$$

in the limit $a^i \rightarrow 0$ for all i .

The log likelihood can be written:

$$h((a^i)_{i=1}^m) = \log p(y^1 \dots y^m) \quad (62)$$

$$= \log \int_s \prod_i \mathcal{N}(y^i - a^i s; 0, (r^i)^2) p(s) ds \quad (63)$$

We then have

$$\frac{\partial h}{\partial a^i} = \left(\frac{1}{h} \frac{\partial h}{\partial a^i} \right) \quad (64)$$

$$= \frac{\int_s -s \frac{(y^i - a^i s)}{r^{i2}} \prod_z \mathcal{N}(y^z - a^z s; 0, (r^z)^2) p(s) ds}{\int_s \prod_i \mathcal{N}(y^i - a^i s; 0, (r^i)^2) p(s) ds} \quad (65)$$

Therefore if $\forall i, a^i = 0$, we get:

$$\frac{\partial h}{\partial a^i}(0) = \frac{\int_s -s \frac{(y^i)}{r^{i2}} p(s) ds}{\int_s p(s) ds} = 0 \quad (66)$$

since $\int_s s p(s) ds = 0$.

Therefore a stationary point is reached when the scale goes to infinity. We show that this stationary point is not a maximum of the log-likelihood.

$$\frac{\partial h}{\partial a^i a^j}(0) = \left(\frac{1}{h} \frac{\partial h}{\partial a^i a^j} - \frac{1}{h^2} \frac{\partial p}{\partial h^i} \frac{\partial p}{\partial h^j} \right)(0) \quad (67)$$

$$= \left(\frac{1}{h} \frac{\partial h}{\partial a^i a^j} \right)(0) \quad (68)$$

If $i \neq j$ we get:

$$\frac{1}{h} \frac{\partial h}{\partial a^i a^j} = \quad (69)$$

$$\frac{\int_s s^2 \frac{(y^i - a^i s)}{r^{i2}} \frac{(y^j - a^j s)}{r^{j2}} \prod_z \mathcal{N}(y^z - a^z s; 0, (r^z)^2) p(s) ds}{\int_s \prod_z \mathcal{N}(y^z - a^z s; 0, (r^z)^2) p(s) ds} \quad (70)$$

$$\implies \left(\frac{1}{h} \frac{\partial h}{\partial a^i a^j} \right)(0) = \frac{y^i y^j}{(r^i r^j)^2} \quad (71)$$

since $\int_s s^2 p(s) ds = 1$.

If $i = j$ we get:

$$\frac{1}{h} \frac{\partial h}{\partial a^i a^i} \quad (72)$$

$$= \frac{\int_s (s^2 \frac{(y^i - a^i s)^2}{(r^i)^4} + \frac{2a^i s - y^i}{r^{i2}}) \prod_z \mathcal{N}(y^z - a^z s; 0, (r^z)^2) p(s) ds}{\int_s \prod_z \mathcal{N}(y^z - a^z s; 0, (r^z)^2) p(s) ds} \quad (73)$$

$$\implies \left(\frac{1}{h} \frac{\partial h}{\partial a^i a^i} \right) (0) = \frac{(y^i)^2}{(r^i)^4} - \frac{y^i}{r^{i2}} \quad (74)$$

since $\int_s s^2 p(s) ds = 1$.

With $a^i = 0$, y^i has variance $(r^i)^2$ and zero mean. So, in expectation the Hessian is positive definite. Therefore $\forall i, a^i = 0$ is a minimum of the loglikelihood and a maximum of the negative log-likelihood.

Therefore at the minima, there exists a finite γ^i . Therefore σ^i is also finite since the ratio must remain bounded. But since the precisions are constrained to be in $[\mu^2, 1 - m\mu^2]$ if σ^i is finite $\forall i, \sigma^i$ is finite. Therefore $\forall i, \gamma^i$ is finite since the ratio must remain bounded.

This shows that as the parameters get close to the border of the definition set of loss (4), the loss either goes to $+\infty$ or goes towards a local maximum. Therefore, there exists parameters $(\gamma_j^i)_{i=1, j=1}^{m, k}, (\lambda_j^i)_{i=1, j=1}^{m, k}, (\sigma_j)_{j=1}^k$ such that $(\Gamma^i (A^i)^{-1})_{i=1}^m, (\lambda_j^i)_{i=1, j=1}^{m, k}, (\sigma_j)_{j=1}^k$ is a well defined local minima of the loss (4).

C Closed form MMSE estimator: detailed computations

$$\begin{aligned} p(\mathbf{x}, \mathbf{s}) &= p(\mathbf{x}|\mathbf{s})p(\mathbf{s}) = \prod_{i=1}^m p(\mathbf{x}^i|\mathbf{s})p(\mathbf{s}) \\ &\propto \exp\left(-\sum_{i=1}^m \sum_{j=1}^k \frac{(\lambda_j^i)^2 m}{2(\sigma_j)^2} (y_j^i - s_j)^2\right) p(\mathbf{s}) \\ &\propto \prod_{i=1}^m \prod_{j=1}^k \left[\exp\left(-\frac{(\lambda_j^i)^2 m}{2(\sigma_j)^2} (y_j^i - s_j)^2\right) \delta(s_j) \right] \\ &= \prod_{j=1}^k \exp\left(-\frac{m}{2(\sigma_j)^2} \sum_i (\lambda_j^i)^2 ((y_j^i - \tilde{s}_j)^2)\right) \exp\left(-\frac{m}{2(\sigma_j)^2} (\tilde{s}_j - s_j)^2\right) \delta(s_j) \\ &\propto \prod_{j=1}^k \exp\left(-\frac{m}{2(\sigma_j)^2} (\tilde{s}_j - s_j)^2\right) \delta(s_j) \end{aligned}$$

We then have

$$\exp\left(-\frac{m}{2(\sigma_j)^2} (\tilde{s}_j - s_j)^2\right) \delta(s_j) \quad (75)$$

$$= \sqrt{2\pi \frac{\sigma^2}{m}} \mathcal{N}(s_j; \tilde{s}_j, \frac{(\sigma_j)^2}{m}) \sum_{\alpha \in \{\frac{1}{2}, \frac{3}{2}\}} \mathcal{N}(s_j, 0, \alpha) \quad (76)$$

$$= \sqrt{2\pi \frac{\sigma^2}{m}} \sum_{\alpha \in \{\frac{1}{2}, \frac{3}{2}\}} \mathcal{N}(s_j; \tilde{s}_j, \frac{(\sigma_j)^2}{m}) \mathcal{N}(s_j, 0, \alpha) \quad (77)$$

$$= \sqrt{2\pi \frac{\sigma^2}{m}} \sum_{\alpha \in \{\frac{1}{2}, \frac{3}{2}\}} \mathcal{N}(\tilde{s}_j; 0, \alpha + \frac{\sigma^2}{m}) \mathcal{N}(s_j; \frac{\alpha \tilde{s}_j}{\alpha + \frac{(\sigma_j)^2}{m}}, \frac{\frac{(\sigma_j)^2}{m} \alpha}{\alpha + \frac{(\sigma_j)^2}{m}}) \quad (78)$$

$$\propto \sum_{\alpha \in \{\frac{1}{2}, \frac{3}{2}\}} \mathcal{N}(\tilde{s}_j; 0, \alpha + \frac{\sigma^2}{m}) \mathcal{N}(s_j; \frac{\alpha \tilde{s}_j}{\alpha + \frac{(\sigma_j)^2}{m}}, \frac{\frac{(\sigma_j)^2}{m} \alpha}{\alpha + \frac{(\sigma_j)^2}{m}}) \quad (79)$$

where we use in (78) the fact that:

$$\mathcal{N}(x; y, \nu) \mathcal{N}(x, 0, \alpha) = \mathcal{N}(y; 0, \nu + \alpha) \mathcal{N}(x; \frac{\alpha y}{\alpha + \nu}, \frac{\nu \alpha}{\alpha + \nu}) \quad (80)$$

We now prove 80:

$$\mathcal{N}(x; y, \nu)\mathcal{N}(x, 0, \alpha) = \frac{\exp\left(-\frac{(x-y)^2}{2\nu}\right) \exp\left(-\frac{x^2}{2\alpha}\right)}{\sqrt{2\pi\nu} \sqrt{2\pi\alpha}} \quad (81)$$

$$= \frac{1}{\sqrt{2\pi\nu}\sqrt{2\pi\alpha}} \exp\left(-\frac{\alpha(x-y)^2 + \nu x^2}{2\alpha\nu}\right) \quad (82)$$

$$= \frac{1}{\sqrt{2\pi\nu}\sqrt{2\pi\alpha}} \exp\left(-\frac{\alpha(x^2 - 2xy + y^2) + \nu x^2}{2\alpha\nu}\right) \quad (83)$$

$$= \frac{1}{\sqrt{2\pi\nu}\sqrt{2\pi\alpha}} \exp\left(-\frac{x^2(\alpha + \nu) - 2x(\alpha y) + \alpha y^2}{2\alpha\nu}\right) \quad (84)$$

$$= \frac{1}{\sqrt{2\pi(\nu + \alpha)}\sqrt{2\pi\frac{\nu\alpha}{\nu + \alpha}}} \exp\left(-\frac{x^2 - 2x\frac{\alpha y}{\alpha + \nu} + \frac{\alpha y^2}{\alpha + \nu}}{2\frac{\alpha\nu}{\alpha + \nu}}\right) \quad (85)$$

$$= \frac{1}{\sqrt{2\pi(\nu + \alpha)}\sqrt{2\pi\frac{\nu\alpha}{\nu + \alpha}}} \exp\left(-\frac{\left(x - \frac{\alpha y}{\alpha + \nu}\right)^2 - \left(\frac{\alpha y}{\alpha + \nu}\right)^2 + \frac{\alpha y^2}{\alpha + \nu}}{2\frac{\alpha\nu}{\alpha + \nu}}\right) \quad (86)$$

$$= \frac{1}{\sqrt{2\pi(\nu + \alpha)}\sqrt{2\pi\frac{\nu\alpha}{\nu + \alpha}}} \exp\left(-\frac{\left(x - \frac{\alpha y}{\alpha + \nu}\right)^2}{2\frac{\alpha\nu}{\alpha + \nu}}\right) \exp\left(-\frac{-\alpha^2 y^2 + (\alpha + \nu)\alpha y^2}{2\alpha\nu(\alpha + \nu)}\right) \quad (87)$$

$$= \frac{1}{\sqrt{2\pi(\nu + \alpha)}\sqrt{2\pi\frac{\nu\alpha}{\nu + \alpha}}} \exp\left(-\frac{\left(x - \frac{\alpha y}{\alpha + \nu}\right)^2}{2\frac{\alpha\nu}{\alpha + \nu}}\right) \exp\left(-\frac{\nu\alpha y^2}{2\alpha\nu(\alpha + \nu)}\right) \quad (88)$$

$$= \mathcal{N}\left(x; \frac{\alpha y}{\alpha + \nu}; \frac{\alpha\nu}{\alpha + \nu}\right)\mathcal{N}(y; 0, \alpha + \nu) \quad (89)$$

D Derivation of relative gradient and Hessian w.r.t W^i in EM

We use the relative gradient \mathcal{G}^{W^i} and \mathcal{H}^{W^i} defined by $\mathcal{C}(W^i + \varepsilon W^i) = \mathcal{C}(W^i) + \langle \varepsilon | \mathcal{G}^{W^i} \rangle + \frac{1}{2} \langle \varepsilon | \mathcal{H}^{W^i} \rangle$. We get:

$$\mathcal{C}(W^i + \varepsilon W^i) = \sum_{i=1}^m [-\log(|W^i|) - \log(|I_k + \varepsilon|) - \log(\mathcal{N}(\mathbf{y}^i + \varepsilon \mathbf{y}^i; \mathbf{s}; \Sigma^i))] + const \quad (90)$$

$$= \mathcal{C}(W^i) - \text{tr}(\varepsilon) + \frac{1}{2} \text{tr}(\varepsilon^2) \quad (91)$$

$$+ \frac{1}{2} [\langle \varepsilon \mathbf{y}^i | (\Sigma^i)^{-1} (\mathbf{y}^i - \mathbf{s}) \rangle + \langle (\mathbf{y}^i - \mathbf{s}) | (\Sigma^i)^{-1} \varepsilon \mathbf{y}^i \rangle + \langle \varepsilon \mathbf{y}^i | (\Sigma^i)^{-1} \varepsilon \mathbf{y}^i \rangle] + o(\|\varepsilon\|^2) \quad (92)$$

$$= \mathcal{C}(W^i) - \sum_a \varepsilon_{a,a} + \frac{1}{2} \sum_{a,b} \varepsilon_{a,b} \varepsilon_{b,a} \quad (93)$$

$$+ \sum_{a,b} \varepsilon_{a,b} [(\Sigma^i)^{-1} (\mathbf{y}^i - \mathbf{s}) (\mathbf{y}^i)^\top]_{a,b} + \frac{1}{2} \sum_{a,b} \varepsilon_{a,b} [(\Sigma^i)^{-1} \varepsilon \mathbf{y}^i (\mathbf{y}^i)^\top]_{a,b} + o(\|\varepsilon\|^2) \quad (94)$$

$$= \mathcal{C}(W^i) - \sum_a \varepsilon_{a,a} + \frac{1}{2} \sum_{a,b} \varepsilon_{a,b} \varepsilon_{b,a} \quad (95)$$

$$+ \sum_{a,b} \varepsilon_{a,b} [(\Sigma^i)^{-1} (\mathbf{y}^i - \mathbf{s}) (\mathbf{y}^i)^\top]_{a,b} + \frac{1}{2} \sum_{a,b,d} \varepsilon_{a,b} (\Sigma^i)_{a,a}^{-1} \varepsilon_{a,d} [\mathbf{y}^i (\mathbf{y}^i)^\top]_{d,b} + o(\|\varepsilon\|^2) \quad (96)$$

So:

$$\mathcal{G}_{a,b}^{W^i} = -\delta_{a,b} + [(\Sigma^i)^{-1} (\mathbf{y}^i - \mathbf{s}) (\mathbf{y}^i)^\top]_{a,b} \quad (97)$$

and

$$\mathcal{H}_{a,b,c,d}^{W^i} = \delta_{a,d} \delta_{b,c} + \delta_{a,c} \frac{y_b^i y_d^i}{\Sigma_a^i} \quad (98)$$

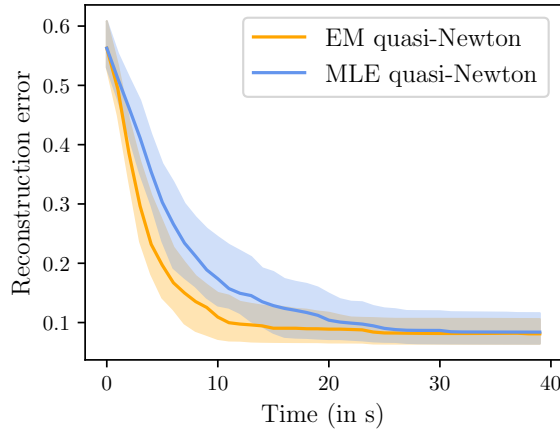


Figure 7: **Convergence plot**: Median reconstruction error as a function of time. Error bars display the first and last quartiles.

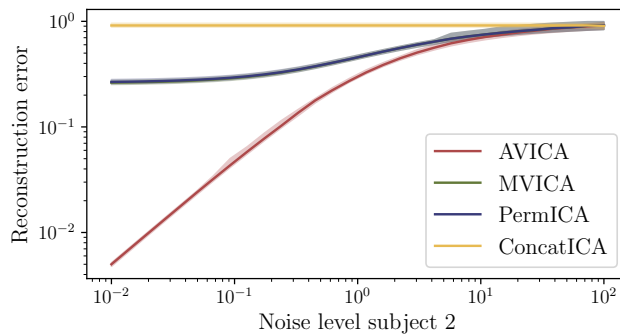


Figure 8: **Synthetic experiment - Adaptive scaling**: Reconstruction error as a function of the noise variance of subject 2 using only one component. The noise variance of subject 1 is fixed to 100. Error bars represent first and last deciles.

E Additional experiments

E.1 Further convergence plots

At each iteration, we record the estimated sources $\hat{\mathbf{s}}$. The true sources \mathbf{s} and the estimated sources are then normalized so that they have unit variance. Then, using the Hungarian algorithm they are matched and the sign is flipped so that for each source j , s_j and \hat{s}_j have maximum correlation. Then, the reconstruction error is defined as $\frac{1}{k} \sum_{j=1}^k (1 - \mathbb{E}[s_j \hat{s}_j])$.

We run this experiment 100 times with different seeds. We provide in Figure E.1 the median reconstruction error in function of time.

E.2 Comparative study of the adaptive scaling of MVICA and AVICA

Both MVICA and AVICA have the ability to put less weights on subjects that are noisier. MVICA can do so by adjusting the scaling of the unmixing matrix of each subject while AVICA can in addition make use of its estimate of the noise precisions. Proposition 1 shows that AVICA is identifiable up to a scaling and permutation. In contrast MVICA is identifiable up to a permutation only as the noise variance is fixed to 1. Therefore with MVICA there is a trade-off between scaling the data so that the noise has variance 1 or scaling the data so that the sources have the correct variance. Such issues do not occur in AVICA.

In order to show this, we consider one-dimensional data x^1 and x^2 which are both a scaled version of a common source. We add to subject x^1 a noise of variance 100 while we add a noise of variance between $10^{-2} \dots 10^2$ to the second subject. We apply ICA algorithms on these data and measure the reconstruction error as $1 - \mathbb{E}[s\hat{s}]$ between the true source s and the source \hat{s} given by the algorithms after normalization to unit variance. Results given in Fig 8 show that AVICA puts more weight on the less noisy subject yielding a good estimate of the common sources while other methods are not able to make use of the less noisy subjects.

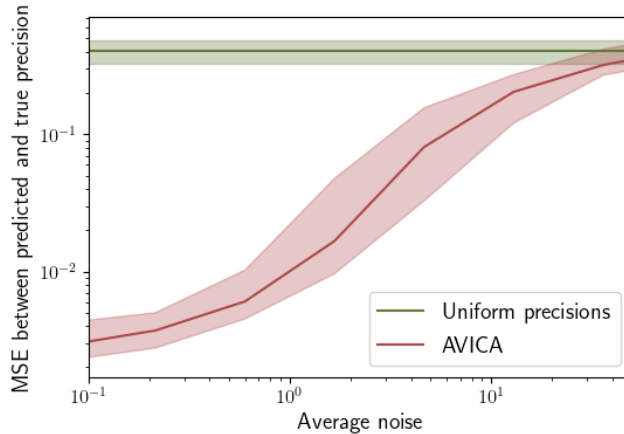


Figure 9: **Synthetic experiment - Error on precisions:** L2 distance between true and estimated precisions.

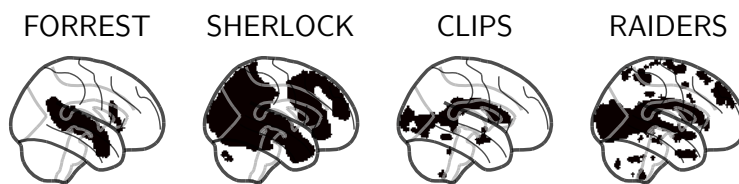


Figure 10: ROI chosen in the reconstruction experiment in section 4.3

E.3 Parameter identification

Adaptive multiViewICA MMSE estimator computes the shared response estimate as a weighted average of individual responses where the weights corresponds to the precisions.

In this experiment we measure the ability of Adaptive multiViewICA to recover the correct precisions using the same data as in the synthetic experiment in section 4.2.

We compute the reconstruction error between the true precisions $\lambda_j^{1^2} \dots \lambda_j^{m^2}$ and the estimated precisions $\widehat{\lambda}_j^{1^2} \dots \widehat{\lambda}_j^{m^2}$ using the formula $\sum_{i=1}^m \sum_{j=1}^k ((\lambda_j^i)^2 - (\widehat{\lambda}_j^i)^2)^2$ and show the result in Figure 9 after applying the hungarian algorithm to deal with permutation indeterminacies.

Figure 9 shows that the precisions obtained using Adaptive multiViewICA are accurate. For comparison we give the reconstruction error between the true precisions and the uniform assignment $(\lambda_j^i)^2 = \frac{1}{m}$.

E.4 ROI chosen for the reconstruction experiment

We report in figure 10 the ROIs used in the reconstruction experiment in section 4.3.

E.5 Stability of spatial ICA decompositions on HCP Rest

In this experiment, we study the stability of spatial ICA decompositions on rest fMRI data with respect to the group of subjects chosen to perform the decomposition. We use the HCP rest dataset Van Essen et al. (2013).

We randomly divide subjects into two groups of 100 subjects and perform spatial ICA separately. We match the components of the two groups using the hungarian algorithm and compute the mean ℓ_2 distance across components. The experiment is repeated 10 times. We report the median value in Figure 11. Error bars represent the first and last quartiles.

We see that AVICA and MVICA yield more stable decompositions than other methods. In particular, AVICA exhibits best performance with 10 components.

E.6 MEG Phantom

We demonstrate the usefulness of AVICA on MEG data. The first experiment uses data collected with a realistic head phantom, which is a plastic device mimicking real electrical brain sources. Thirty two current dipoles positioned at different locations can be switched on or off.

We select N_d dipole at random among the set of 32 dipoles where N_d varies from 2 to 20. We view each dipole as a subject and therefore have $m = N_d$. We only consider the 102 magnetometers.

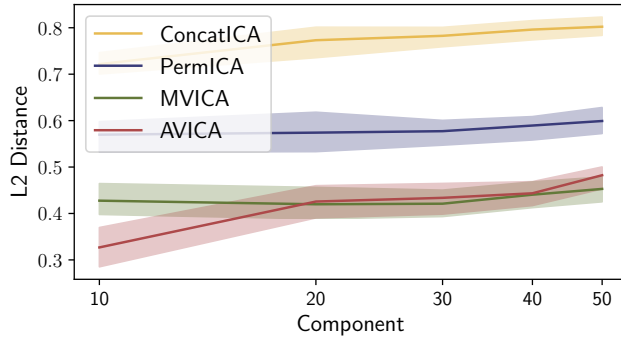


Figure 11: **Stability of spatial ICA decompositions on fMRI rest data:** We divide subjects into two groups of 100 subjects and perform spatial ICA separately. We match the components of the two groups and report the mean ℓ_2 distance across components. The experiment is repeated 10 times. We report the median value. Error bars represent the lower and upper quartile.

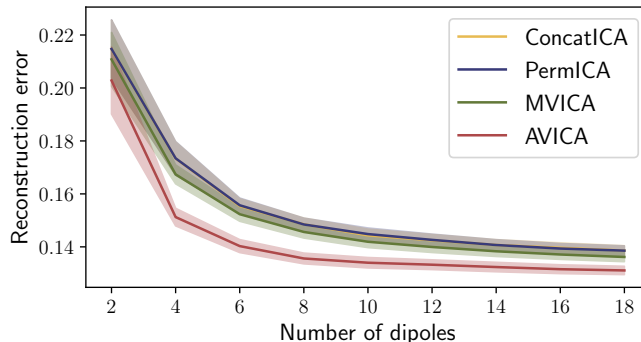


Figure 12: **MEG Phantom:** Reconstruction error between estimated and true source

An epoch corresponds to 3s of MEG signals where a dipole is switched on for 0.4s with an oscillation at 20 Hz and a peak-to-peak amplitude of 200 nAm. This yields a matrix of size $p \times n$ where $p = 102$ is the number of sensors, and n is the number of time samples. We have access to 100 epochs per dipole. For each dipole, we chose 2 epochs at random among the set of 100 epochs and concatenate them in the temporal dimension.

We apply algorithms to our data to extract $k = 5$ shared sources. As we know the true source (the timecourse of the dipole), we can compute the reconstruction error of each source as the squared norm of the difference between the estimated source and the true source, after normalization to unit variance and fixing the sign. We only retain the source of minimal error.

This metric is reported in Figure 12 when the number of dipoles considered N_d varies. Adaptive multiViewICA outperforms other methods.

E.7 MEG CamCAN Timecourses

We display in Figure 13 the sources corresponding to the 6 chunks of data.

As we can see, the sources corresponding to the same stimuli are very similar over repetitions.

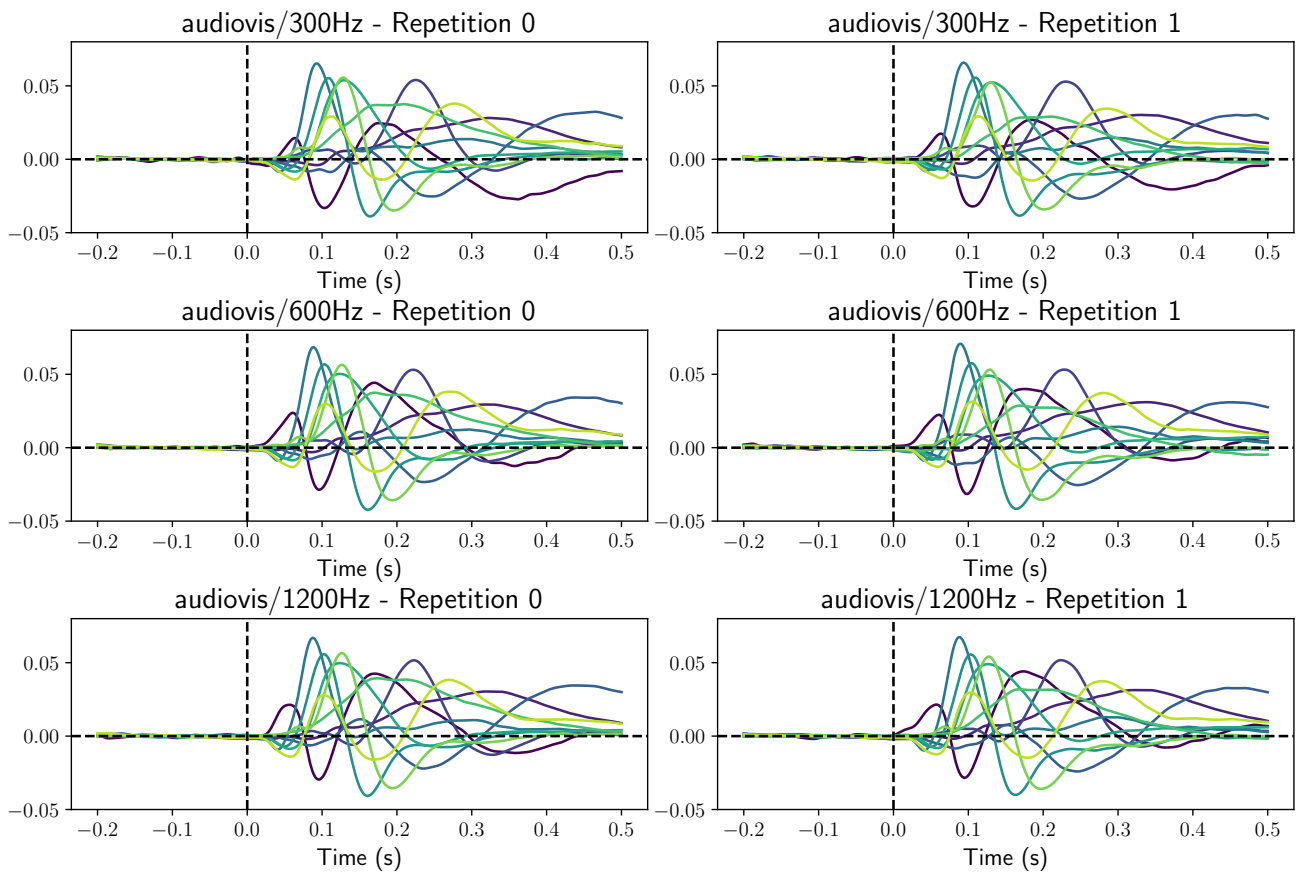


Figure 13: **CamCAN MEG**: Timecourse of 10 shared sources recovered by Adaptive multiViewICA

E.8 Detailed CamCAN sources

For each subject, sources are localized using the sLORETA algorithm Pascual-Marqui et al. (2002) Then, they are registered to a common reference brain and averaged across subjects. We plot the sources obtained using Adaptive multiViewICA and their localization below.

